Comparative effects of digested human milk and infant formulas on peptide transport and gut barrier function in infant- and adult-like Caco-2/HT29-MTX models

Food Research International 235 (2026) 119071

Contents lists available at ScienceDirect

Food Research International

journal homepage: www.elsevier.com/locate/foodres

Comparative effects of digested human milk and infant formulas on peptide transport and gut barrier function in infant- and adult-like Caco-2/HT29-MTX models

Francesca Bietto [a,b], Simona Cirrincione [c], Cristina Gómez-Marín [d], Beatriz Miralles [d], Francesco Romaniello [e], Elena Arranz [d,f], Cristina Lamberti [c], Simona Lucia Bavaro [c], Laura Cavallarin [c], Eva Rath [g], Alice J. Lucey [b], Linda Giblin [a,*]

[a] Teagasc Food Research Centre, Moorepark, Fermoy, Co. Cork, Ireland
[b] School of Food and Nutritional Sciences, University College Cork, Cork, Ireland
[c] Institute of the Science of Food Production (ISPA) – National Research Council, Grugliasco, TO 10095, Italy
[d] Institute of Food Science Research CIAL (CSIC-UAM), Madrid, Spain
[e] National Metrological Institute of Italy (INRIM), Torino 10135, Italy
[f] Sección Departamental de Ciencias de la Alimentación, Universidad Autónoma de Madrid (UAM), Madrid, Spain
[g] Chair of Nutrition and Immunology, School of Life Sciences, Technische Universität München, Freising, Germany

ARTICLE INFO

Keywords:
Human milk
Infant formula
Gut barrier
Peptide transport
Bioactive peptides
Intestinal epithelial cells
Intestinal permeability
In vitro gastrointestinal digestion
Caco-2/HT29-MTX, INFOGEST

ABSTRACT

Early postnatal nutrition is critical for gut barrier maturation, yet infant formulas only partially replicate the functional benefits of human milk. Using infant- and adult-like Caco-2/HT29-MTX models, this *in vitro* study compared the effects of gastrointestinal digested human milk, dairy-, soya-, and amino acid–based infant formulas on gut barrier integrity and peptide transport. Barrier function was assessed by transepithelial electrical resistance and occludin–actin colocalization, while amino acid and peptide transport were profiled by liquid chromatography plus mass spectrometry.

In the infant-like model, human milk uniquely enhanced occludin–actin co-localization ($P < 0.05$) and increased the abundance of basolateral bioactive peptides. Amino acid–based infant formula significantly increased occludin fluorescence intensity in infant-like monolayers but reduced transepithelial electrical resistance (TEER) in adult-like monolayers. For all digested foods, peptide transport and diversity were significantly greater in infant-like than in adult-like monolayers, with human milk promoting the highest basolateral peptide load.

These findings demonstrate distinct functional differences between human milk and infant formulas in their interaction with the gut barrier. They also underscore the importance of using age-appropriate *in vitro* models for accurately evaluating dietary effects during early life, highlighting the need for further research to optimize infant nutrition strategies.

1. Introduction

Human milk is the gold standard of human infant nutrition, offering not only complete nourishment but also bioactive compounds that support the health and development of the infant (Brockway et al., 2024). In the intestinal tract of the infant, human milk plays a critical role in promoting gut barrier integrity (Carr et al., 2021), reducing paracellular permeability (Catassi et al., 1995), and shaping the intestinal microbiome (Bode, 2012; Pannaraj et al., 2017).

The infant gut barrier is characterized by high permeability during early development. In several domestic species (e.g., calves, piglets, lambs), the neonatal small intestine can absorb intact colostral immunoglobulins, predominantly IgG, thereby establishing systemic passive immunity (Weström et al., 2020). In humans, systemic passive immunity is acquired primarily before birth through active FcRn-mediated transplacental transfer of maternal IgG (Atyeo & Alter, 2021). Nevertheless, the human neonatal gut barrier remains highly permeable in early infancy with significantly higher lactulose permeability (Kosek et al.,

* Corresponding author.
E-mail address: Linda.Giblin@teagasc.ie (L. Giblin).

https://doi.org/10.1016/j.foodres.2026.119071
Received 24 November 2025; Received in revised form 19 March 2026; Accepted 2 April 2026
Available online 8 April 2026

2017) and a higher lactulose-to-mannitol ratio than adults, indicating predominance of paracellular over transcellular transport pathways (Johnston et al., 2000; Musa et al., 2019; Weaver et al., 1984). These permeability traits are linked to lower expression of tight junction proteins (e.g., Occludin- OCLN, Zonulin-1- ZO1, Tight Junction Protein 1-TJP1) and higher levels of the permeability-enhancing claudin-2 (CLDN2) in early life. Intestinal barrier maturation, as reflected by decreasing permeability, continues for up to 15 months after birth in human infants (Kosek et al., 2017). Human milk promotes this maturation process, as observed by lactulose: mannitol experiments (Catassi et al., 1995). The World Health Organization recommends exclusive breastfeeding in the first 6 months of life (World Health Organization, 2014). However, the choice to breastfeed is deeply personal and can be shaped by a variety of factors (Blum, 1999). Infant formula (IF) can be used as an alternative or supplement for the first 12 months of life (UNICEF. and W. H. O., 2003). Dairy-based IF is the most widely used. Soya-based IF offers a plant-based alternative, whereas highly hydrolysed and amino acid (AA)-based IF are designed for infants with severe protein allergies or gastrointestinal disorders (Martin et al., 2016). Although nutritionally similar to human milk, IFs do not replicate the health benefits of human milk on the gut barrier, particularly in promoting gut maturation, integrity, and reducing the risk of necrotizing enterocolitis (Colaizy et al., 2016; Lucas & Cole, 1990; Quigley et al., 2024).

The Codex Alimentarius (CXS 72–1981), established by FAO/WHO, sets international standards for the composition, safety, and labelling of IF products (Codex Alimentarius Commission, 1981). In the EU, Regulation (EU) 2016/127 governs IF, mandating detailed compositional criteria (European Commission, 2016), including adequate protein or AAs, to meet the requirements for growth and development. During digestion, proteins are broken down into peptides and free AAs (Korhonen & Pihlanto, 2006). While free AAs are absorbed directly via specific transporters (Bröer, 2008), small peptides are taken up either via peptide transporters or by paracellular diffusion (Hevia et al., 2023). Many of these peptides can exert bioactive effects on the gut barrier (Dold et al., 2025; Korhonen & Pihlanto, 2006). Moreover, a recent systematic review also confirms that milk-derived proteins and peptides can be detected in the bloodstream of human infants post-ingestion, supporting their potential for systemic bioactivity (Biondi Ryan et al., 2025).

To study nutrient digestion in the infant gut, the Ménard et al. protocol offers an in vitro static gastrointestinal digestion method to track digestion under infant conditions (Ménard et al., 2018). Recent studies with this protocol have demonstrated comparable overall protein digestibility between human milk and dairy IF, as assessed by free amino acid release, molecular weight distribution, and peptidomic analysis (Komatsu et al., 2024; Sánchez-Hernández et al., 2021). Polarized Caco-2/HT29-MTX monolayers are a well-established in vitro model of the adult gut barrier (Kleiveland, 2015). Absorption of peptides from human milk and IF has been evaluated using Caco-2 monolayers following in vitro digestion of these matrices (Bavaro et al., 2021; Liang et al., 2022). Although few studies have evaluated the effects of human milk–derived peptides on Caco-2/HT29-MTX monolayers' gut barrier properties, peptides released from IF during digestion increased mRNA transcripts of mucins within these monolayers (Dold et al., 2025).

The substantial differences between the infant and adult gut barrier in terms of permeability warrant an age-appropriate transient model to simulate gut maturation and nutrient uptake from human milk and from the various IFs. However, in vitro gut barrier models for this life stage remain scarce. Current models, including cell lines (Sun et al., 2008; Vergauwen, 2015), enteroids (Noel et al., 2021), and animal models (Sangild et al., 2014), are constrained by physiological, ethical, or scalability limitations. In our previous work, we developed a reversible gut barrier model by treating Caco-2/HT29-MTX monolayers with 0.8 mM sodium glycodeoxycholate (GDC). These monolayers mirrored key aspects of the in vivo infant barrier, showing significantly reduced TEER, increased paracellular permeability (a 1.63-fold increase in lactulose transport), and altered OCLN localization, without inflammation or cytotoxicity (Bietto et al., 2025). This phenotype aligns with in vivo observations showing that intestinal permeability in young infants is approximately 55% higher at 3 months than at 15 months of age (Kosek et al., 2017). Reduced OCLN localization is consistent with reports of lower OCLN and ZO1 expression in neonatal intestine compared to adults (Gleeson et al., 2021; Holmes et al., 2006). Moreover, GDC treatment increased acidic mucin production and alkaline phosphatase activity, features consistent with the predominance of acidic mucus in early life (Johansson et al., 2011; Macierzanka et al., 2014) and elevated intestinal alkaline phosphatase reported in neonates (Cummins et al., 1988). Importantly, barrier integrity recovered within 4 h following GDC removal, confirming reversibility and supporting a model of adaptive, non-pathological permeability (Bietto et al., 2025).

The objective of this in vitro study was to compare human milk with dairy IF, soya IF, and AA IF using infant-like models of gastrointestinal digestion and gut barrier function. Specifically, we aimed (i) to evaluate the effects of these foods on structural tight junction remodeling, tracking OCLN localization in infant- and adult-like Caco-2/HT29-MTX monolayers, and (ii) to quantify free AAs and identify individual dietary peptides in the basolateral chambers of these monolayers.

2. Materials and methods

A schematic overview of the experimental workflow and analytical pipeline is provided in Supplementary Fig. 8.

2.1. Materials

Dairy-based, soya-based IF, and AA-based IF were shop-bought. The dairy-based infant formula contained cow's milk proteins as the primary protein source, the soya-based formula contained soy protein isolate, and the amino acid–based formula contained free amino acids as the sole nitrogen source. All products were manufactured within the European Union and complied with the compositional requirements for infant formula as defined by Commission Delegated Regulation (EU) 2016/127 and Codex Alimentarius (CXS 72–1981). Human milk samples were collected from six healthy lactating women approved by the ethics committee of the Hospital Universitario Virgen de las Nieves (Granada, Spain) and registered on ClinicalTrials.gov (accessed 15 April 2019; NCT02811172). Mature milk (≥17 days postpartum) from each donor was pooled to create a composite sample. Rabbit gastric extract 15 (RGE 15; lot no. 1201) was obtained from Lipolyltech. A bicinchoninic acid (BCA) assay kit was purchased from Pierce® (Ireland). XT MES Running Buffer, Precision Plus Protein™ Unstained Standard were sourced from Bio-Rad. AccQ-Tag Ultra Derivatization Kit, Ultra AA Analysis Column, and AA Hydrolysate Standard were purchased from Waters® (MA, USA). Transwell inserts with polyester permeable membranes were obtained from Sarstedt Group (Germany). CellTiter 96® AQueous One Solution Cell Proliferation Assay was supplied by Promega. Rabbit anti-Occludin (Sigma-Aldrich), Alexa Fluor 488 Donkey anti-Rabbit (A-21206), Alexa Fluor 555 Phalloidin (A-34055), DAPI (268298), and ProLong™ Glass Antifade Mountant (P36980) were supplied by Thermo Fisher Scientific (MA, USA). Strata C18-E SPE Solid Phase Extraction and Luna C18 column were purchased from Phenomenex (Torrance, USA). Human intestinal epithelial cell lines Caco-2 (EACC 86010202) and HT29-MTX-E12 (EACC 12040401) were purchased from the European Collection of Cell Culture (UK). All other reagents were purchased from Sigma-Aldrich, unless otherwise stated.

2.2. Simulated static infant gastrointestinal digestion (SGID)

IFs were reconstituted according to the manufacturers' instructions to simulate realistic preparation and feeding conditions for infants. Accordingly, 4.3 g of dairy- and soya-based IF powder and 4.5 g of amino

acid–based IF powder were dissolved in 30 mL of MilliQ water, as specified by the manufacturer for each formulation. Human milk samples were thawed at 4 °C. Crude protein content was determined in duplicate using the Kjeldahl method (FOSS Scrubber 2501 / Kjeltec Sampler 8420 / Kjeltec 8400) on freeze-dried samples. Crude protein was calculated using the standard factor (N × 6.25).

Simulated gastrointestinal digestion (SGID) was performed according to the Ménard et al., 2018 protocol (Ménard et al., 2018). An oral phase was not included. Initially, 5 mL of reconstituted IF or human milk was mixed with 2.94 mL of infant simulated gastric fluid containing 268 U/mL RGE 15 (pepsin activity determined in-house = 596 U/mg). Milli-Q water (5 mL) subjected to the same digestion conditions served as a negative control. This control was included to assess potential contributions from digestive enzymes in the absence of a food matrix. The pH was brought to 5.3 with 1 M HCl. Samples were incubated for 1 h at 37 °C in a shaking incubator (100 rpm). To stop the gastric phase, pH was raised to 7 with 1 M NaOH. For the intestinal phase, 4.88 mL of simulated intestinal fluids containing 16 U/mL pancreatin (lot no. SLCM8903; trypsin activity determined in-house = 8.9 U/mg) and 3.1 mM bovine bile (lot no. SLBV1780; concentration of bile salts = 440 g/mol) were added to the gastric phase. The pH was decreased to 6.6 with 1 M HCl. The samples were incubated again for 1 h at 37 °C in a shaking incubator. Digestion was then stopped by adding the protease inhibitor 4-(2-aminoethyl)benzenesulfonyl fluoride hydrochloride, dissolved in MilliQ water at a final concentration of 1 mM, along with Orlistat, dissolved in ethanol at a final concentration of 0.1 mM. The digesta were aliquoted and stored at −20 °C until use. Samples were collected at 3 time points: G0, collected immediately after mixing the matrix with simulated gastric fluid, gastric enzymes, and adjusting to 5.3, followed by immediate alkalinisation to inactivate gastric enzymes, with no incubation and therefore no proteolysis; G60, collected at the end of the gastric digestion; and I60, collected at the end of the intestinal digestion. G0 serves as food entering the gastric phase.

Each food was digested on 3 separate occasions ($n = 3$).

2.3. SDS-page

Undigested IF and human milk, as well as samples collected at defined phases of digestion (G0, G60, and I60), were analyzed using SDS-PAGE with 12% Bis-tris–polyacrylamide gels (Criterion XT, Bio-Rad, Hercules, California, USA). Protein content was determined using a bicinchoninic acid (BCA) assay kit, following the manufacturer's instructions. Dairy, soya, and human milk samples were diluted at a protein concentration of 0.8 mg/mL in loading buffer and heated at 95 °C for 5 min. The AA IF contains no intact proteins; therefore, dilution factors were adjusted at each digestion stage to ensure that the total material loaded per lane was comparable to that of dairy IF and soya IF. The resulting dilution factors applied to AA IF were: undigested sample = 1:10.25; G0 = 1:12.33; G60 = 1:9, and I60 = 1:3.44. SGID H_2O, containing digestive enzymes but no food matrix, was loaded undiluted.

The loading buffer was 0.05 M Tris-HCL pH 6.8, SDS 1.6% w:v, glycerol 8% w:w, Bromophenol blue 0.002% w:v, β-mercaptoethanol 2% v:v. Precision Plus Protein™ Unstained Standard(15 μL) was loaded as the M_w standard. Electrophoresis was performed at 150 V for 60 min with XT MES running buffer, and gels were stained overnight with InstantBlue™ solution followed by de-staining with Milli-Q water.

2.4. Total nitrogen content by o-phthaldialdehyde (OPA) assay

The degree of protein hydrolysis was measured through the concentration of free NH_2 groups, determined by the o-phthaldialdehyde (OPA) assay (Nielsen et al., 2001). The G0, G60, and I60 samples were defrosted on ice, precipitated with 5% trichloroacetic acid (0.5 mL of sample in 0.83 mL of TCA), and centrifuged for 30 min at 1000 *g*. The supernatants were then diluted 1:1 (dairy, soya IF, and human milk G0 and G60), 1:4 (I60), or 1:9 (AA IF G0, G60) in a 0.1 mol/L borate solution. Dilution factors were adjusted to account for differences in free amino group concentration across digestion stages and formulations, ensuring all measurements fell within the linear detection range of the OPA assay. The OPA reagent was prepared with 0.1 mol/L borate, 10% SDS, 40 g/L OPA in ethanol, and 200 g/L N-Acetyl-L-Methionine Ethyl Ester. Samples (8 μL) were transferred into a UV 96-well plate and incubated for 10 min at 30 °C in the dark with 232 μL OPA solution. Absorbance at 340 nm was measured using a microplate reader (PowerWave XS, BioTek Instruments, Winooski, Vermont, USA). A standard curve of glutamic acid (0–8 mmol/L) was used for quantification. Hydrolysis % was calculated as follows:

Hydrolysis (%) = 100 - [(mmol NH_2 G0 / mmol NH_2 I0) × 100].

2.5. Size exclusion chromatography (SEC)

Digesta samples (I60) were first clarified by centrifugation at 10,000 ×*g* for 10 min at 4 °C. The resulting supernatant was diluted 1:1 and filtered through a 0.22 μm nylon syringe filter. A 20 μL aliquot was injected into two TSKgel columns connected in series (TSKgel G2000SW, 7.5 mm × 30 cm; TSKgel G2000SWXL, 7.8 mm × 30 cm) with a TSKgel SW guard column (7.5 mm × 7.5 cm) upstream. SEC was performed on a Waters HPLC system (Waters 2695 separation module) equipped with a Waters 2487 dual-wavelength absorbance detector set to 214 nm. Separation was achieved by isocratic elution at 0.7 mL/min for 55 min, using a mobile phase of 0.1 M phosphate buffer (pH 6.7) containing 0.1 M Na_2SO_4 and 10% (*v*/v) methanol.

Molecular-size calibration was carried out by applying the same conditions to a series of standards spanning the protein–peptide range: bovine serum albumin (67 kDa), equine carbonic anhydrase (29 kDa), β-lactoglobulin (18.4 kDa), α-lactalbumin (14.4 kDa), cytochrome *c* (12.4 kDa), bacitracin (1.4 kDa), H-Tyr-Leu-OH (0.29 kDa) and phenylalanine (0.17 kDa). Retention times of these standards were plotted against the logarithm of their molecular weights to generate a calibration curve, which was then used to estimate the size distribution of analytes present in the digesta samples.

2.6. Free and total AAs analysis in the digested samples

Free and total AAs in digested samples were quantified using an AccQ-Tag derivatization UPLC method, which is suitable for acid-hydrolysed samples and enables parallel determination of free and total amino acid pools.

Digested samples (I60) were defrosted on ice, and methanol was added for a final concentration of 80% to precipitate proteins (5 mL final volume). Each sample was centrifuged at 1000 *g* for 30 min. The supernatant (220 μL) was subjected to SpeedVac evaporation (SC200, Savant) to eliminate methanol. To quantify free AAs, the pellet was re-suspended in 500 μL 0.1 mM HCl. To quantify total AAs, the pellet was hydrolysed in 6 M HCl for 15 h at 110 °C in a glass vial. Cys (10 and 1 mmol/L) was also hydrolysed to quantify the derivative forms (Cys2). An internal standard of 25 mM (final concentration) Norvaline was added to the samples prior to hydrolysis. All samples were derivatized using the AccQ-Tag Ultra Derivatization Kit following the manufacturer's instructions. Briefly, the samples were neutralized, filtered with a 0.2 μm nylon filter, mixed with 70 μL AccQ•Tag Ultra Borate Buffer and 20 μL AccQ•Tag Ultra reagent, and incubated at 55 °C for 10 min. The derivatized samples were separated using, and an ACQUITY Ultra Performance UPLC® (Waters Corporation, USA) equipped with a tunable ultraviolet/visible (TUV) detector and a flow cell. Separation was performed with AccQ•Tag Ultra AA Analysis Column (Eluent 1 = AccQ•Tag Ultra Eluent A, Eluent 2 = AccQ•Tag Ultra Eluent B; flow rate = 0.7 mL/min; injection volume = 1 μL). The quantification was performed based on a standard three-point curve (AA Hydrolysate Standard). The Empower software (version3.7.0, Waters Corporation) was used to acquire, process, report, and manage chromatographic information.

2.7. Cell culture

Caco-2 and HT29-MTX cell lines were cultured as previously described for intestinal epithelial co-culture models (Hubatsch et al., 2007; Kleiveland, 2015). Caco-2 and HT29-MTX cell lines were cultured in 75-cm^2 tissue culture flasks maintained at 37 °C, 5% CO_2, in a humidified atmosphere. Following thawing, the cells underwent three passages before use. Unless otherwise stated, cells were maintained in 'complete DMEM', consisting of Dulbecco's Modified Eagle Medium (DMEM, D5796) supplemented with 10% heat-inactivated fetal bovine serum (FBS, F7524), 100 U/mL Penicillin-Streptomycin (P4333), and 2.5 μg/mL amphotericin B (A2942). Additionally, for HT29-MTX cells and for co-culture monolayers, 1% MEM Non-essential AA Solution (M7145) was added to complete DMEM. Cells were passaged at 80% confluence every 4–5 days using 0.25% Trypsin-EDTA solution (T4049). After trypsinization, cells were stained with trypan blue and counted with the TC20 cell counter (Bio-Rad, USA). Experiments were performed using Caco-2 cells between passages 21–25 and HT29-MTX cells between passages 64–68.

2.8. MTS assay

Cell viability, following exposure to digested samples, was assessed using the CellTiter 96® AQueous One Solution (MTS) assay, following the manufacturer's instructions and previously reported protocols for Caco-2-based intestinal models (Bavaro et al., 2021).

Digested samples collected at the intestinal phase (I60) were defrosted on ice, diluted in HBSS (1:4, 1:9, 1:14, 1:19), filter-sterilized (0.2 μm syringe filter), and warmed to 37 °C. Caco-2/HT29-MTX were seeded in a 96-well plate (Corning® CellBIND®) at a concentration of 5×10^4 cells/well and incubated for 24 h. Cells were then washed twice with HBSS and incubated for 2 h with diluted digested samples (150 μL). After the incubation period, the digesta was removed. Cells were washed twice with HBSS and incubated for 1 h at 37 °C with the MTS reagent (100 μL), diluted 1:10 in HBSS following the CellTiter 96® AQueous One Solution Cell Proliferation Assay kit instructions. Absorbance was read at 490 nm in a multi-plate reader (BioTek Cytation 5 multimode reader). Cell viability was expressed as a percentage of HBSS-treated control cells. Viability of control cells consistently exceeded 88% of cells maintained in complete DMEM.

2.9. Caco-2/HT29-MTX monolayers exposure to GDC and digesta

A 90:10 ratio (Caco-2:HT29-MTX) was seeded in the apical chamber (500 μL) of 12-well plates containing polyester permeable-membrane inserts (Sarstedt Group), reaching a final density of 6×10^4 cells/well. The basolateral chamber received 1.5 mL of complete DMEM with 1% MEM Non-essential AAs. The culture medium was refreshed every two days. Transepithelial electrical resistance (TEER) was monitored weekly using a Millicell-ERS Voltohmmeter (Merck Millipore, USA), with background TEER values obtained from Transwells without cells. Following our protocol (Bietto et al., 2025), monolayers were washed twice on day 24 and incubated with serum-free DMEM D1145 for 16 h. Only monolayers exhibiting TEER values $>800\ \Omega \times cm^2$ were selected for experiments (Bietto et al., 2025). Monolayers were washed with HBSS and pre-equilibrated in DMEM D1145 (0.4 mL apical, 1.5 mL basolateral) for 30 min at 37 °C. To create the infant-like barrier, monolayers were incubated for 2 h at 37 °C with GDC (0.8 mM). Firstly, GDC (4 mM) was freshly prepared and sterile-filtered in DMEM D1145. A volume of 100 μL was added to the apical compartment with 400 μL DMEM. TEER values were recorded at 0 and 2 h. Control 'adult-like' monolayers were treated with DMEM D1145 during the same timeframe. Following treatment, monolayers were washed twice and incubated with HBSS (0.4 mL apical, 1.5 mL basolateral) for 15 min at 37 °C for acclimatization. Digested IF and human milk samples were thawed on ice, diluted 1:2 in HBSS, sterile-filtered (0.2 μm PES syringe filters), and prewarmed to 37 °C. Subsequently, 100 μL sample was added to the apical chamber, achieving a final ratio of 1:14. TEER values were recorded before and after the 2 h incubation period. Apical and basolateral media were collected after the incubation period (T2-apical, T2-basolateral) and stored at −20 °C for subsequent AA and peptide analysis. Monolayers were fixed for immunofluorescence and confocal microscopy.

2.10. Immunofluorescence and confocal microscopy

Monolayers were washed twice with PBS and fixed for 30 min at room temperature by adding 500 μL of 75% ethanol (prepared in PBS) into the apical chamber. Monolayers were then washed twice with PBS and kept at 4 °C in PBS until use (max 1 week). Monolayers were permeabilized with 75% acetone in PBS for 3 min at room temperature, washed, and incubated for 30 min at room temperature with blocking solution (1% BSA in PBS). The primary antibody (Rabbit anti-Occludin, Sigma Aldrich) was added (1:149 dilution) in blocking solution (150 μL) and incubated overnight at 4 °C. Fixed monolayers were washed twice with PBS. Then, secondary antibody (A-21206, Alexafluor 488 Donkey anti-rabbit, Thermo Fisher Scientific;1:499 dilution) plus actin binder, phalloidin 555 (binds to F-actin, A-34055, Alexa Fluor 555 Phalloidin, Thermo Fisher Scientific; 1:499 dilution), was added to the blocking solution (150 μL). Monolayers were incubated for 1 h in the dark at room temperature, washed three times with PBS, and incubated with DAPI (268,298, Merk; 1:4999 dilution in MilliQ water) for 2 min, in the dark at room temperature to stain cell nuclei. The permeable supports of the Transwell plates were excised with a scalpel and mounted on a microscopy glass slide with 40 μL of mounting media (ProLong™ Glass Antifade Mountant, Thermo Fisher Scientific).

Samples were imaged using STED and FALCON (FLIM) coupled to an inverted DMi8 microscope (Leica Microsystems, Germany) equipped with a white light laser (440–790 nm). The objective used was Plan-Apochsomat 63×/1.4 Oil DIC N2. Pinhole size was set to 85.6 nm. Images were captured with Power HyD S detectors (Leica) at a pixel size of 0.7 μm in the Z dimension and 0.18 μm in the X and Y dimensions. Alexa Fluor 488 acquisition parameters were: 512–542 nm (emission range), 0.4 μs (dwell time), 3.9 (gain), and 56.89% (laser intensity). Alexa Fluor 555 acquisition parameters were: 565–605 (emission range), 0.4 μs (dwell time), 35.5 (gain), and 68.10% (laser intensity). DAPI acquisition parameters were: 450–490 nm (emission range), 0.4 μs (dwell time), 5 (gain), and 14.67% (laser intensity) Line average of 2 was applied to every channel.

Fiji/ImageJ software was used to determine OCLN fluorescence intensity, number of nuclei, colocalization with actin, orthogonal view, and monolayer thickness. The intensity threshold was determined using the Otsu algorithm for intensity quantification. The colocalization between OCLN (Alexa 488) and actin (Alexa 555) was calculated using the JACoP Fiji/ImageJ plugin, with thresholds set to 7000 for Alexa 488 and 8000 for Alexa 555. For each test sample, 3 slides and 3 pictures per slide were analyzed. For figure presentation purposes, brightness and contrast were adjusted uniformly across the entire images to improve the visualization of OCLN localization. These adjustments were applied only to the images used for illustration and were not applied to the raw image files used for quantitative fluorescence intensity or colocalization analyses.

2.11. Free AAs transported in the basolateral side

Free AAs were quantified in the T2-basolateral compartment using an untargeted UHPLC-HRMS method optimized for hydrophilic compounds. This method was selected for its high sensitivity at low amino acid concentrations. Digesta samples were analyzed in parallel for reference. The separation was performed on a Thermo Vanquish Flex UHPLC system using a Thermo Accucore™ Amide-HILIC column (150 × 2.1 mm, 2.6 μm particle size), maintained at 30 °C. Sample (1 μL) was

injected and separated under a flow rate of 400 μL/min using a binary gradient composed of solvent A (H_2O with 10% ammonium formate, 20 mM, pH 2.8) and solvent B (ACN with 10% ammonium formate, 20 mM, pH 2.8). The gradient started at 0% A and ramped to 60% A over 22 min, followed by re-equilibration back to initial conditions for a total run time of 45 min.

UHPLC was coupled to a high-resolution Orbitrap mass spectrometer (Q Exactive Plus, Thermo Fisher Scientific) via a Heated Electrospray Ionization (H-ESI) source. Full MS data were acquired in positive ionization mode with the following parameters: spray voltage 2.80 kV, capillary temperature 150 °C, sheath gas 35 AU, auxiliary gas 10 AU, sweep gas 1 AU, and auxiliary gas heater temperature 150 °C. The S-Lens RF level was set to 50.0. Full MS scans were acquired at a resolution of 70,000, with an AGC target of 3.0e6 and maximum injection time of 100 ms, across an *m/z* range of 65–250. Data-dependent MS/MS (dd-MS^2) was performed using an isolation window of 2 m/z, resolution 17,500, collision energy of 20 eV, AGC target of 5.0×10^4, and maximum IT of 50 ms, with an intensity threshold of 4.0×10^4.

Quantification of AAs was based on external calibration curves generated at 7 concentration levels ranging from 0.5 to 80 mg/L. Isotopically labelled internal standards were used at 10 mg/L, and the peak areas of each analyte were normalized to its corresponding internal standard.

2.12. Peptide profiling by UHPLC-HRMS/MS

2.12.1. Sample preparation for UHPLC-HRMS/MS

Peptides from digesta, T2-apical and T2-basolateral compartments were purified using solid-phase extraction (SPE) using STRATA C18-E cartridges (55 μm, 70 Å, 1 mL/50 mg). Digesta samples were diluted to match the concentration applied in cell exposure experiments. Briefly, the digesta was diluted 1:2 (*v*/v) with Milli-Q water and filtered using a 0.2 μm PES syringe filter. A further 1:4 (v/v) dilution in Milli-Q water was performed to achieve a 1:14 dilution in line with cell exposure studies. A 483 μL aliquot was then processed using C18 SPE and reconstituted in 120 μL Milli-Q H_2O. For T2-apical samples, 2 technical replicates were pooled (1.0 mL total). A 483 μL aliquot was purified using C18 SPE. For T2-basolateral samples, 1.5 mL from each of 2 technical replicates (3.0 mL total) was pooled. A 2.9 mL aliquot was subjected to C18 SPE.

Prior to loading, SPE cartridges were conditioned with 3 × 1 mL methanol and equilibrated with 3 × 1 mL Milli-Q water. Samples were loaded onto the cartridges by gravity flow, followed by washing with 1 mL of 0.5% (*v*/v) methanol in water. Peptides were eluted with 3 × 1 mL methanol.

Eluates were evaporated to dryness using a nitrogen stream at 45 °C. Dried samples were reconstituted in 120 μL Milli-Q water for digesta and T2-apical samples, and in 12 μL Milli-Q water for T2-basolateral samples. All samples were stored at −20 °C until analysis. A 10 μL injection volume was used for UHPLC–HRMS/MS analysis.

2.12.2. UHPLC-HRMS/MS analysis

Peptide analysis was performed using an Orbitrap Q Exactive Plus mass spectrometer (Thermo Fisher Scientific) coupled to a Vanquish Flex UHPLC binary pump system. Separation was achieved on a Luna C18 reversed-phase column (150 × 1 mm, 3 μm of particle size). The mobile phases consisted of 0.1% (*v*/v) formic acid in Milli-Q water (solvent A) and 0.1% (v/v) formic acid in 30% acetonitrile, 70% methanol (solvent B), delivered at a flow rate of 70.0 μL/min. The elution gradient was programmed to increase solvent B from 3% to 50% over 80 min, with 70% in 5 min, 100% in 1 min, and 5 min, then reconditioned at 3% B for 15 min. The injection volume was 2.0 μL. Column temperature was maintained at 55 °C, and the autosampler was set at 4 °C to preserve sample integrity.

UHPLC was coupled to a high-resolution mass spectrometer via an H-ESI source. Full MS data were acquired in positive ionization mode with the following parameters: spray voltage 3.50 kV, capillary temperature 350 °C, sheath gas 35 AU, auxiliary gas 10 AU, sweep gas 1 AU, and auxiliary gas heater temperature 250 °C. The S-Lens RF level was set to 50.0.

Mass spectra were acquired in data-dependent acquisition mode (Full MS-ddMS^2). Full scan spectra were recorded over an *m/z* range of 250–1500 with a resolution of 70,000, an AGC (automatic gain control) target of 3×10^6, and a maximum injection time of 200 ms. Up to 6 of the most intense ions in MS1 were selected for fragmentation in the MS/MS mode. The fragmentation spectra resolution was set at 17,500, with a dynamic exclusion of 10 s and an isolation window of 2.0 m/z. The normalized collision energy was set at 28 (eV), the maximum IT at 110 ms, and the AGC target at 1×10^5.

2.12.3. Peptide identification

Raw data were processed using MaxQuant (v2.6.6.0) (Cox & Mann, 2008) with an unspecific digestion mode and a minimum peptide length of 2 AAs, suitable for naturally occurring peptides. The main search mass tolerance was set to 4.5 ppm for precursors and 20 ppm for fragment ions. Variable modifications included oxidation (M), acetylation (protein N-term), phosphorylation (STY), and pyro-glutamate formation (Q/E). No fixed modifications or enzyme constraints were applied. The "second peptide" and "match between runs" features were enabled, with a match time window of 0.7 min. Label-free quantification (LFQ) was enabled with an LFQ minimum ratio count of 2 and stabilization of large ratios. Intensity normalization was based on FastLFQ.

Database searches were performed against custom UniProtKB FASTA files corresponding to *Bos taurus* (dairy, 402 entries), *Glycine* max (soy, 109 entries), or *Homo sapiens* (human milk, 1142 entries) and a manually added contaminants FASTA file (124 entries), retaining only reviewed sequences. Decoy sequences were automatically generated for FDR estimation using the revert mode. Peptide-spectrum match (PSM), peptide, and protein FDR thresholds were each set to 1%. Additional filtering required a minimum Andromeda score of 40 for modified peptides and a minimum delta score of 6. All MS/MS data were searched using Andromeda, with up to 15 candidate matches per spectrum and deisotoping enabled.

2.12.4. Bioinformatics analysis

Raw and annotated peptide data from MaxQuant output files (evidence.txt, peptides.txt) were post-processed using Python (v3.10) (Python Software Foundation, 2021) within a Google Colab (Google Research, n.d.) environment. Data manipulation and filtering were conducted using pandas (v1.5.3) (McKinney, 2010) and numpy (v1.23.5) (Harris et al., 2020) libraries. Peptides were retained only if they had at least one MS/MS count, belonged to a single protein group, and showed non-zero intensity in ≥2 biological replicates per condition. Peptides identified in T2-apical and T2-basolateral compartments were further filtered to ensure their source protein was also detected in the corresponding digesta dataset. Reverse hits and known contaminants were excluded from all analyses.

Shared and unique peptides were identified using set-based comparisons and classified as follows: peptides detected in only one compartment were labelled "compartment-unique," while those in both were "shared." Within each compartment-unique set, we further classified by age group: an "exclusive" label was used for those peptides that were present in only one age group (Infant or Adult), whereas a "shared" label was used when peptides were present in both. Overlaps were visualized via Venn diagrams using matplotlib-venn (Tretyakov, 2012). For count-based statistics, per-peptide PSM counts across Infant and Adult were subjected to equal-variance *t*-tests. For intensity-based analysis, raw intensities were $\log_2$-transformed, then imputed from a left-shifted normal distribution (mean = μ–1.8σ, σ = 0.3·global σ); per-peptide $\log_2$ means and Welch's t-tests were computed on the imputed data. A parallel workflow was applied to modified peptides (grouped by Sequence + Modification). Significantly enriched peptides ($P < 0.05$)

were annotated by source protein and mapped across compartments.

To assess peptide transformation by brush border enzymes, apical-only peptides were analyzed using a classification pipeline. Assignment of brush-border enzymatic cleavage events was performed using a motif-based in silico prediction approach. Apical peptides were matched to longer digesta-derived precursor sequences using a breadth-first search based on established N- and C-terminal cleavage motifs characteristic of known intestinal brush border peptidases.

The cleavage motifs used for prediction were as follows: Dipeptidyl peptidase-4 /8/9: N-terminal dipeptides, X–P/A; Aminopeptidase N: N-terminal single residues, L/I/V/M/A; Aminopeptidase A: N-terminal E/D; Aminopeptidase B: N-terminal R/K; Enteropeptidase: N-terminal D/E/R/K; Carboxypeptidase A: C-terminal F/L/I/W/Y/V/M; Carboxypeptidase B: C-terminal R/K; Dipeptidyl carboxypeptidase: C-terminal dipeptides, G/S/D; Tripeptidyl peptidase II: N-terminal tripeptides.

Bioactivity annotation was conducted via cross-referencing with BIOPEP (Minkiewicz et al., 2019), the Milk Bioactive Peptide Database (MBPD) (Nielsen et al., 2017), and PeptideRanker (Mooney et al., 2012) (score threshold ≥0.5). Volcano plots were generated using scikit-learn (v1.2.2) (Pedregosa, 2011), matplotlib (Hunter, 2007), and seaborn (Waskom, 2021) for dimensionality reduction and visual inspection of condition-driven separation.

In parallel, digesta peptides were characterized using sequence-derived physicochemical metrics. Peptide length was calculated as the number of amino acid residues per sequence and summarized as discrete distributions and biologically relevant length categories (2–3, 4–10, 11–20, and > 20 residues). Peptide molecular weight was calculated as the sum of the average residue masses plus 1 water molecule (18.01 Da) and summarized into molecular weight ranges (<500, 500–1000, 1000–2000, and > 2000 Da). Peptide hydrophobicity was calculated using the Kyte–Doolittle scale and expressed as mean hydropathy per residue, with distributions summarized into hydrophilic, neutral, and hydrophobic categories. Amino acid composition was determined as the percentage of total amino acid residues.

The same analytical framework was applied to peptides identified in the T2-basolateral compartment. Within each dietary matrix, peptides were classified as common (detected in both infant- and adult-like models) or model-specific (infant-only or adult-only) based on exact sequence matching. Peptide length, molecular weight, hydropathy (Kyte–Doolittle index), net charge at pH 7, amino acid composition, proline content, and terminal residue frequencies were calculated *in silico*. Descriptive statistics (median and interquartile range) were computed, and the proportion of peptides exceeding three amino acids (>3 AAs) was determined.

All outputs were exported using xlsxwriter (McNamara, 2023), and the entire pipeline was modular, script-based, and reproducible.

2.13. Statistical analysis

All experiments were conducted in triplicate or quadruplicate across three separate days, each with technical duplicates or triplicates. Results are expressed as means ± SEM. Statistical analyses for cellular and functional assays were performed using GraphPad Prism 10.4.2 (GraphPad Software, USA), employing one-way ANOVA with Tukey's = multiple comparison test, except for free amino acid profiles in digesta, which were analyzed using Welch's one-way ANOVA followed by pairwise comparisons with Benjamini–Hochberg false discovery rate (FDR). For individual amino acid comparisons reported in the Supplementary Tables, differences among food matrices were analyzed using two-way ANOVA followed by Tukey's multiple comparisons test, as specified in the Supplementary Materials. Statistical significance was defined as $P < 0.05$.

For peptidomic data, statistical analysis was conducted in Python (v3.10) using Welch's *t*-test via the scipy.stats module (Virtanen, 2020). Peptide-level comparisons were based on $\log_2$-transformed intensity values across conditions, and peptides with $P < 0.05$ were considered significantly differentially enriched.

3. Results

3.1. IFs and human milk exhibit similar protein hydrolysis with differences in molecular size distribution and amino acid profiles

Human milk and 3 commercially available IFs (dairy, soya, and AA-based) were subjected to static gastrointestinal digestion adapted to the infant gut (Ménard et al., 2018). Prior to digestion, crude protein content determined by Kjeldahl was 9.41% for dairy IF, 13.25% for soya IF, 14.16% for AA IF (expressed as protein equivalents from free AAs), and 10.11% for human milk. To mimic the in vivo consumption of these liquid foods, the protein content was not standardised before digestion. However, no significant differences in total protein content were found between dairy IF, soya IF, and human milk, at the end of the intestinal phase (3556 ± 314.4 μg/mL, BCA assay, $P > 0.05$, Supplementary Fig. 1 A).

SDS-PAGE revealed distinct digestion patterns. Dairy IF and human milk showed progressive loss of intact proteins such as caseins and α-lactalbumin, with human milk preserving lactoferrin (Supplementary Fig. 1B). Soya IF displayed a diffuse smear indicative of extensive hydrolysis, and AA IF showed no bands, consistent with its composition of free AAs (Supplementary Fig. 1B).

OPA assay confirmed progressive proteolysis across all samples, with similar degrees of hydrolysis (~82–85%) in dairy IF, soya IF, and human milk. AA IF showed higher initial free NH_2 content due to its formulation, which decreased upon dilution during digestion (Fig. 1A).

Size exclusion chromatography at the I60 timepoint (after gastric and intestinal digestion) revealed that digested AA IF consisted almost entirely of <0.5 kDa molecules (88%). In contrast, dairy IF, soya IF, and human milk revealed that the majority (90%) of compounds were < 5 kDa in size. Human milk uniquely retained a small fraction (>5%) of >50 kDa proteins, suggestive of digestion-resistant proteins (Fig. 1B).

To assess potential contributions from the digestion system itself, the simulated digestion water control (SGID H_2O), containing digestive enzymes but no food matrix, was analyzed in parallel. SDS-PAGE of undiluted SGID H_2O confirmed the presence of residual digestive enzymes (rabbit gastric extract and pancreatin). At the same time, size-exclusion chromatography showed a profile dominated by low-molecular-weight components, with the majority below 0.5 kDa (Supplementary Fig. 2 A and B).

To evaluate the nutritional quality of digested proteins, the concentrations of total hydrolyzed (Fig. 1C) and free (Fig. 1D) AAs were quantified in the bioaccessible fraction of the digesta (I60), defined as the methanol-soluble fraction containing protein digestion products released from the food matrix and present in a solubilized, potentially absorbable form (Grundy et al., 2025). These AAs weregrouped as branched-chain AAs (BCAAs), essential AAs (EAAs), and non-essential AAs (NEAAs).

Among digested dairy IF, soya IF, and human milk, total AA concentrations ranged from 357,060.6 ± 4180.8 μmol/L (human milk) to 430,180.2 ± 10,823.3 μmol/L (soya IF), with dairy IF at 394,794.6 ± 8488.2 μmol/L. Digested soya IF had significantly higher total AA content compared to digested human milk ($P < 0.05$). In digested dairy IF, soya IF, and human milk, NEAAs represented the majority of the total pool. EAAs ($P > 0.05$) and BCAA ($P > 0.05$) were similar across these digested samples.

Glutamic acid was the most abundant AA in dairy IF (51,845.7 ± 1325.9 μmol/L), soya IF (62,339.6 ± 14,38.66 μmol/L; $P < 0.05$), and human milk at the I60 timepoint (50,277.0 ± 699.0 μmol/L) (Fig. 1C and Supplementary Table 1 A). Digested dairy IF had the highest leucine (39,956.1 ± 11,45.6 μmol/L; P < 0.05) and lysine content (29,784.0 ± 573.34 μmol/L; $P < 0.05$). Soya IF had the highest arginine (24,264.6 ± 735.9 μmol/L; $P < 0.05$), glycine (50,334.3 ± 656.4 μmol/L; $P < 0.05$), serine (27,974.4 ± 905.7 μmol/L; $P < 0.05$) and aspartic acid content

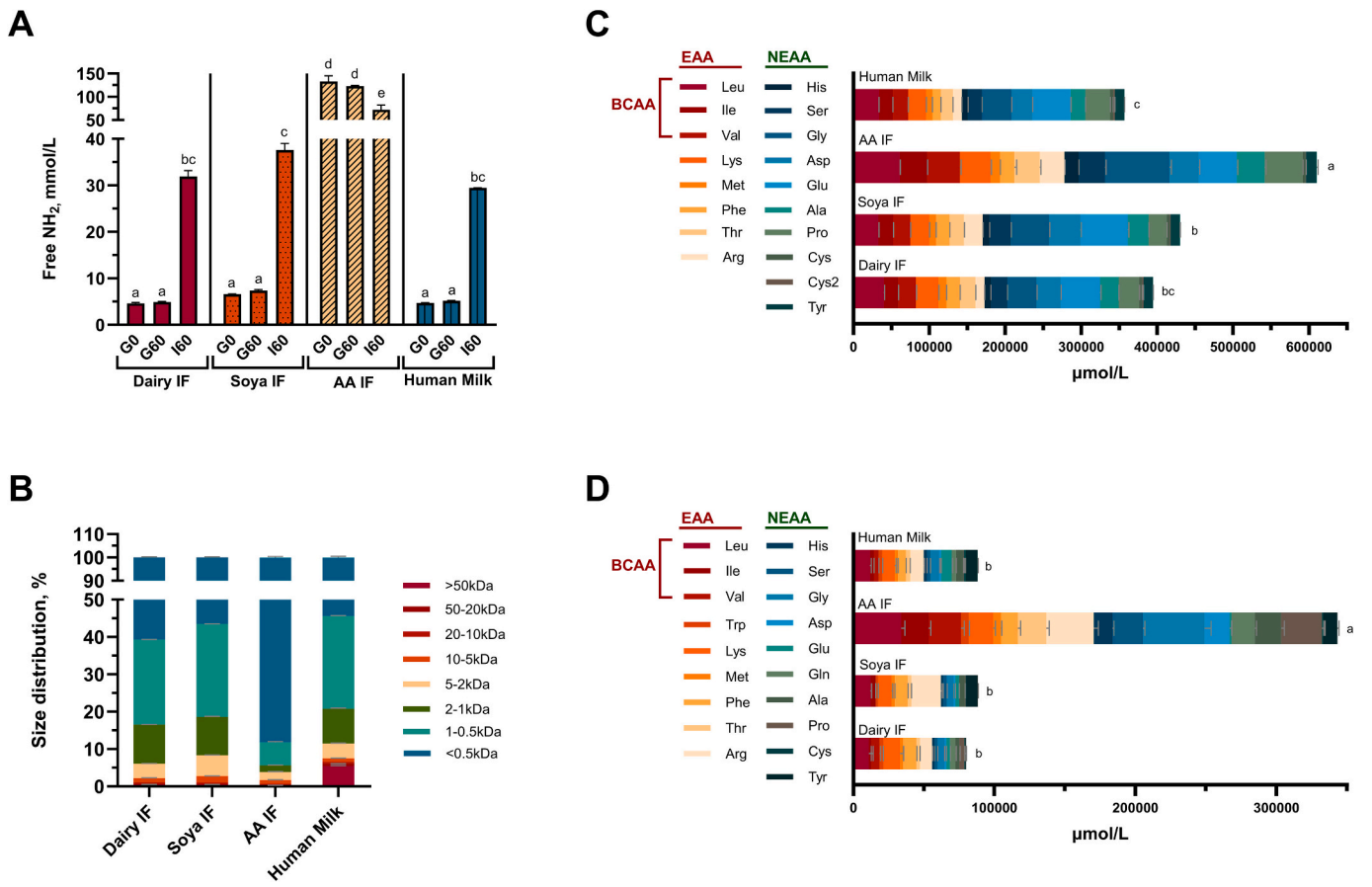

Fig. 1. Infant gastrointestinal digestion of Dairy, Soya and amino acid-based (AA) infant formulas (IF) and Human Milk (A) Degree of protein hydrolysis, assessed by OPA, at G0 (before gastric phase), G60 (after gastric phase) and I60 (after intestinal phase) timepoints. (B) Size exclusion chromatography of the soluble fraction at I60 timepoint. (C) I60 digesta Total amino acids, quantified by UPLC. (D) I60 digesta free amino acids quantified by UPLC. Data represent mean values from three independent digestions performed on separate days. Statistical analysis was performed using one-way ANOVA followed by Tukey's multiple comparisons test (A-C), or (D) Welch's one-way ANOVA followed by pairwise comparisons with Benjamini–Hochberg false discovery rate (FDR) correction. Different letters indicate statistically significant differences ($P < 0.05$). Amino acids are colour-coded as follows: red = branched-chain amino acids (BCAA), red + orange = essential amino acids (EAA), blue/green = non-essential amino acids (NEAA). (For interpretation of the references to colour in this figure legend, the reader is referred to the web version of this article.)

(41,279.4 ± 10,33.28 µmol/L; $P < 0.05$). Digested human milk contained the highest concentration of proline (32,463.9 ± 514.1 µmol/L; $P < 0.05$) (Fig. 1C and Supplementary Table 1 A).

Total free AA values were not significantly different among digested dairy IF (80,016.3 ± 8284.9 µmol/L), soya IF (88,309.6 ± 4960.9 µmol/L), and human milk (88,140.1 ± 5478.3 µmol/L; $P > 0.05$). Free EAAs and BCAA were similar in digested dairy IF, soya IF, and human milk ($P > 0.05$) (Fig. 1D).

Notably, digested soya IF showed significantly higher free arginine compared to dairy IF and human milk (20,914.9 ± 1024.6 µmol/L, $P < 0.05$), while digested human milk had significantly more free glutamic acid (7542.4 ± 588.1 µmol/L) than both dairy IF (2642.8 ± 367.2 µmol/L) and soya IF (2699.9 ± 155.0 µmol/L, $P < 0.05$) (Fig. 1D and Supplementary Table 1C).

Digested AA IF had significantly higher concentrations of AAs across all categories ($P < 0.05$) (Fig. 1 and Supplementary Table 1). Total AAs were 610,221.0 ± 13,721.7 µmol/L, with NEAAs and EAA at 214,226. ± 3090.7 µmol/L and 14,2834.5 ± 1135.39 µmol/L respectively, exceeding all other samples. Free AAs were equally elevated (343,283.8 ± 27,830.0 µmol/L), with glycine, leucine, and arginine ranking as the top three free residues (Supplementary Table 1C).

The total AA content and free AA content of SGID H_2O control were 99,888.9 ± 14,587.4 µmol/L and 25,382.0 ± 8797.2 µmol/L, respectively, indicating minimum AA contribution from digestive enzyme autolysis. In summary, human milk and infant formulas showed similar overall hydrolysis but differed in molecular size distribution and amino acid composition, reflecting matrix-specific digestion patterns. The contribution of amino acids arising from digestive enzyme autoproteolysis is shown in the SGID H_2O control (Supplementary Fig. 2C and D).

3.2. *Digested IFs and human milk maintain infant-like barrier integrity*

To assess the impact of digested IFs and human milk on intestinal barrier integrity, an infant-like epithelial monolayer was treated with digested samples. For comparison purposes Caco-2/HT29-MTX monolayers were included, representing an adult barrier (Hidalgo et al., 1989).

Initially, MTS assay was employed to determine the appropriate dilution to ensure biocompatibility of the digested samples with Caco-2/HT29-MTX co-cultures (Supplementary Fig. 3). Dilutions ≥1:14 of dairy IF, soya IF, AA IF, and human milk did not significantly affect cell viability compared to the SGID H_2O control ($P > 0.05$). In contrast, dilutions ≤1:9 resulted in a significant decrease in viability ($P < 0.05$). Therefore, 1:14 was selected as the highest non-toxic concentration for subsequent experiments.

To create an infant-like barrier, day 25 Caco-2/HT29-MTX monolayers were treated with 0.8 mM GDC, leading to the expected and

significant reduction in TEER (Bietto et al., 2025) from 1165 ± 11.85 Ω × cm^2 to 412.15 ± 18.98 Ω × cm^2 (experiment baseline TEER) (Fig. 2A). Following 2 h exposure to digesta (T2), infant-like cultures maintained stable TEER values regardless of milk formulation (Fig. 2A; $P > 0.05$).

At baseline (T0), adult-like monolayers had a TEER value of 1010.90 ± 96.96 Ω × cm^2. No significant TEER reduction was observed in adult-like monolayers with the digested dairy IF, soya IF, or human milk samples for 2 h (T2) ($P > 0.05$). Treatment with digested AA IF resulted in a significant drop in TEER in adult-like monolayers (Fig. 2B; $P < 0.05$).

3.3. Digested human milk enhances OCLN–actin co-localization in infant-like monolayers

To investigate whether exposure to digested IFs or human milk promotes gut barrier maturation, tight junction protein OCLN was labelled in Caco-2/HT29-MTX co-cultures under infant- and adult-like conditions after 2 h treatment. OCLN localization was assessed by fluorescence intensity normalized to nuclei count (Fig. 3, Supplementary Fig. 4). Its spatial relationship with the actin cytoskeleton was evaluated through co-localization analysis (Fig. 4).

Infant-like monolayers treated with digested human milk exhibited a distinct pattern of OCLN distribution, characterized by focal accumulation of OCLN at cell junctions, visible as dot-like structures (Fig. 3A, white arrows), which were not present in adult monolayers. In the adult-like model, treatment with dairy IF, AA IF, or human milk digesta resulted in lower OCLN intensity than with soya IF ($P < 0.05$). Digested AA IF significantly increased OCLN fluorescence intensity in infant-like monolayers, compared to digested dairy IF ($P < 0.05$).

When comparing infant- vs. adult-like conditions within each treatment, baseline OCLN fluorescence under HBSS control was significantly lower in infant-like monolayers (120,127 ± 9556) than in adult-like monolayers (201,627 ± 2397; $P < 0.05$, Fig. 3B). Similarly, soya IF treatment induced significantly higher OCLN intensity in adult-like monolayers compared to intensity in the infant-like model ($P < 0.05$).

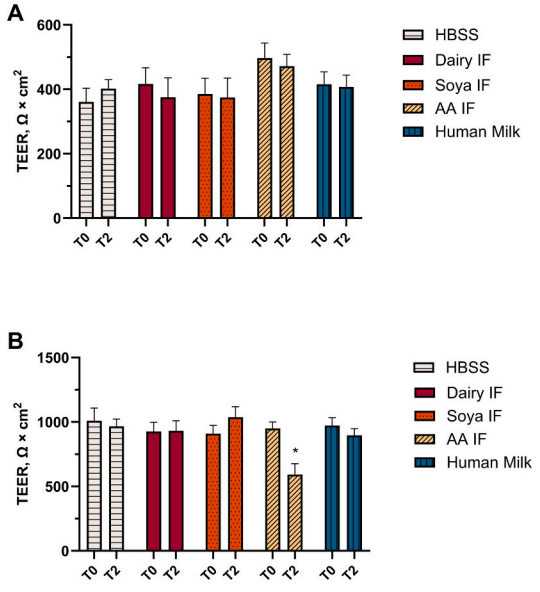

Fig. 2. Transepithelial electrical resistance (TEER) of Caco-2/HT29-MTX monolayers treated with digested infant formulas (IF) or Human Milk. (A) Infant-like and (B) adult-like monolayers (90:10) were exposed for 2 h to digested Dairy IF, Soya IF, amino acid-based (AA) IF, and Human Milk (1:15 in HBSS). TEER at day 25 = 1165 ± 11.85 Ω × cm^2. T0 = Before digesta addiction; T2 = post-treatment. Data are mean ± SEM from six biological replicates (three digestions × two exposures × duplicate wells; $n = 12$). One-way ANOVA with Tukey's test; *$P < 0.05$ vs. HBSS.

To further examine the interaction between OCLN and the actin cytoskeleton, Pearson's and Manders' co-localization coefficients were calculated for OCLN and actin signals (Fig. 4). Pearson's coefficient, which reflects the degree of spatial alignment between OCLN and the actin cytoskeleton, was significantly increased by digested human milk on infant-like monolayers compared to the infant HBSS control (0.32 ± 0.02 vs. 0.37 ± 0.01; $P < 0.05$, Fig. 4A). In contrast, both soya IF and human milk significantly reduced Pearson's coefficient in the adult-like model relative to HBSS ($P < 0.05$).

When comparing across developmental models, HBSS-treated infant monolayers exhibited a significantly lower Pearson's coefficient than adult monolayers (0.27 ± 0.02 vs. 0.40 ± 0.01; $P < 0.05$). Interestingly, both soya IF and human milk significantly increased this coefficient in the infant-like model compared to their adult counterparts ($P < 0.05$), suggesting increased spatial alignment between OCLN and actin under infant conditions.

These findings were supported by Manders' coefficient M1, which reflects the fraction of the OCLN signal that overlaps with actin. M1 was increased in infant-like monolayers treated with soya IF compared to HBSS control ($P < 0.05$, Fig. 4B). In the adult model, M1 was significantly reduced following exposure of monolayers to dairy IF and human milk compared to HBSS control ($P < 0.05$, Fig. 4B). Among all treatments, HBSS-treated infant monolayers displayed significantly lower M1 values than adults (0.33 ± 0.03 vs. 0.65 ± 0.04; $P < 0.05$, Fig. 4B).

M2 (fraction of actin overlapping OCLN) was less biologically informative, as actin is broadly distributed and its overlap with OCLN does not specifically reflect tight junction structure. Nevertheless, M2 was significantly reduced in soya and AA IF groups for infant and dairy and AA IF for adult compared to HBSS (infant coefficient = 0.14 ± 0.03; adult coefficient = 0.25 ± 0.04, $P < 0.05$, Supplementary Fig. 5). No significant difference was found in M2 for adult and infant monolayer with HBSS treatment.

Interestingly, orthogonal views of z-stack images revealed a significant increase in monolayer thickness, reflective of greater cell height, in our infant-like model with HBSS treatment versus the standard Caco-2/HT29-MTX monolayer with HBSS (13.54 ± 0.34 μm vs. 12.12 ± 0.41 μm; $P < 0.05$) (Supplementary Fig. 6).

3.4. AA IF shows the highest basolateral free AAs levels

Fig. 5 depicts the free AA concentration found in the basolateral compartment of Caco-2/ HT29-MTX monolayers after 2 h exposure to digesta (T2-basolateral). Supplementary Tables 2 A and B report the specific concentrations and statistical comparisons for all free AAs measured in the T2-basolateral compartment. Across all conditions, the five most abundant AAs present in the T2-basolateral samples were lysine, aspartic acid, arginine, threonine, and serine. These five AAs accounted for approximately 50–58% of the total free AAs found in the T2-basolateral compartment across all samples.

In the infant model, treatment with AA IF resulted in a mean free AAs concentration of 8.275 ± 0.362 mg/L, which was higher ($P < 0.05$) than that observed for soya IF (6.444 ± 0.335 mg/L), dairy IF (6.634 ± 0.279 mg/L), and human milk (6.915 ± 0.326 mg/L) treatments. In the adult-like model, treatment with AA IF again led to the highest free AAs levels (7.712 ± 0.360 mg/L), exceeding those from soya IF (6.182 ± 0.094 mg/L), dairy IF (5.728 ± 0.015 mg/L), and human milk (6.275 ± 0.308 mg/L) treatments.

Interestingly, the total amount of free AAs found in the T2-basolateral side was significantly higher in the infant-like model than in the adult for dairy IF (6.64 ± 0.09 vs. 5.73 ± 0.01 mg/L; $P < 0.05$), driven largely by increased transport of glycine (0.27 ± 0.02 mg/L) and serine (0.62 ± 0.11 mg/L) in the infant model ($P < 0.05$). Supplementary Fig. 7 shows the total free AA concentrations in the T2-basolateral compartment of the HBSS control condition, which were not significantly different ($P > 0.05$) between infant-like (3.41 ± 0.52 mg/L) and adult-like (3.97 ± 0.17 mg/L) monolayers. Importantly, these

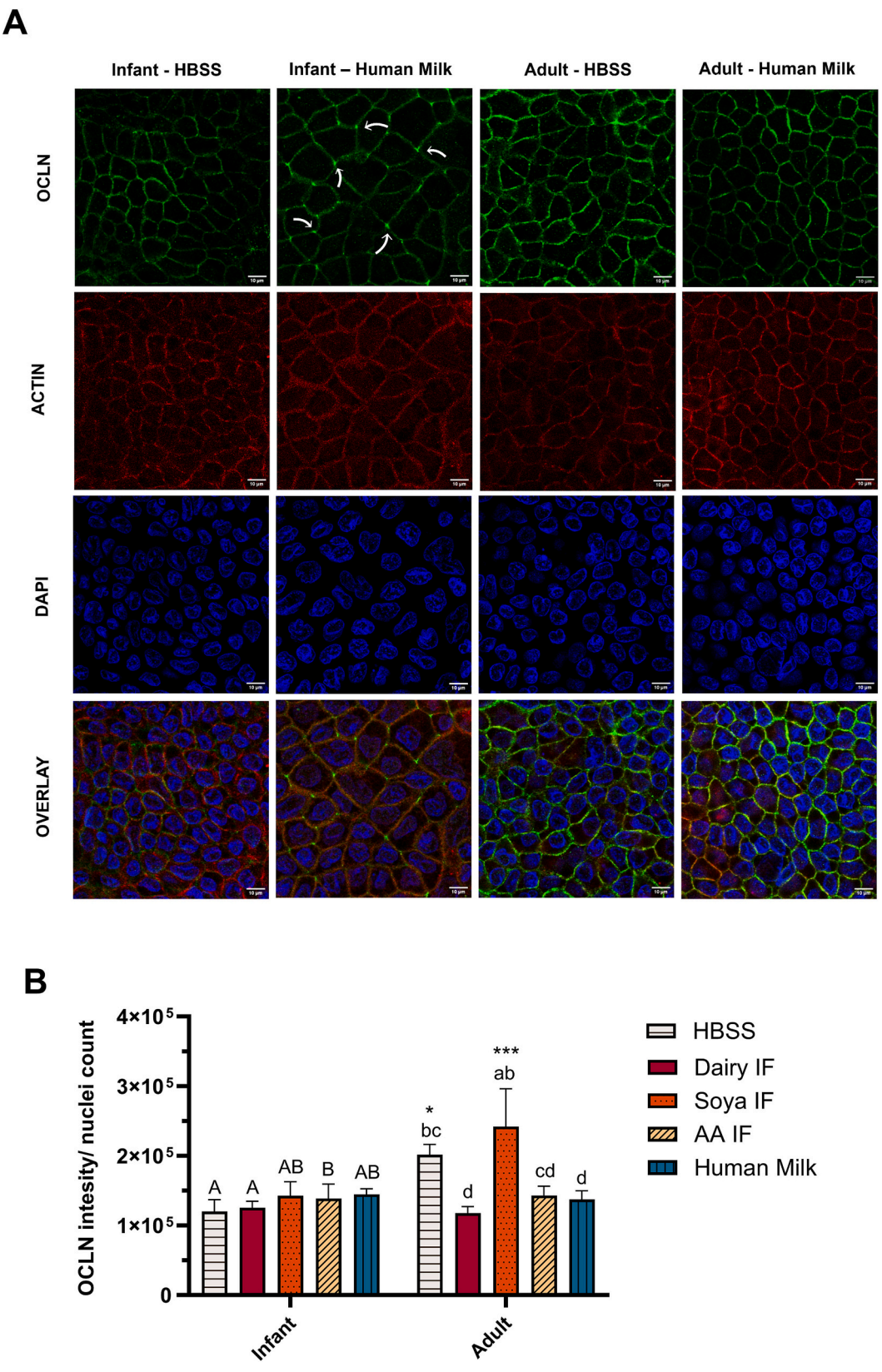

Fig. 3. Occludin (OCLN) localization in infant and adult-like Caco-2/HT29-MTX monolayers treated with digested Human Milk. Monolayers (90:10) were cultured for 25 days and treated for 2 h with HBSS (control) or digested Human Milk. (A) Representative confocal images showing OCLN (green), actin (red), and nuclei (blue); white arrows highlight membrane OCLN with Human Milk. Scale = 10 μm. (B) OCLN fluorescence intensity normalized to nuclei count. Data are mean ± SEM from three biological replicates ($n = 9$). One-way ANOVA with Tukey's test: different letters indicate significant differences within infant (uppercase) or adult (lowercase) models; asterisks indicate significant differences between infant and adult models within the same treatment (*$P < 0.05$; ***$P < 0.001$). Fluorescence intensity and co-localization analysis was performed on raw image files. Brightness and contrast were then adjusted equally across the entire image for visualization purposes. (For interpretation of the references to colour in this figure legend, the reader is referred to the web version of this article.)

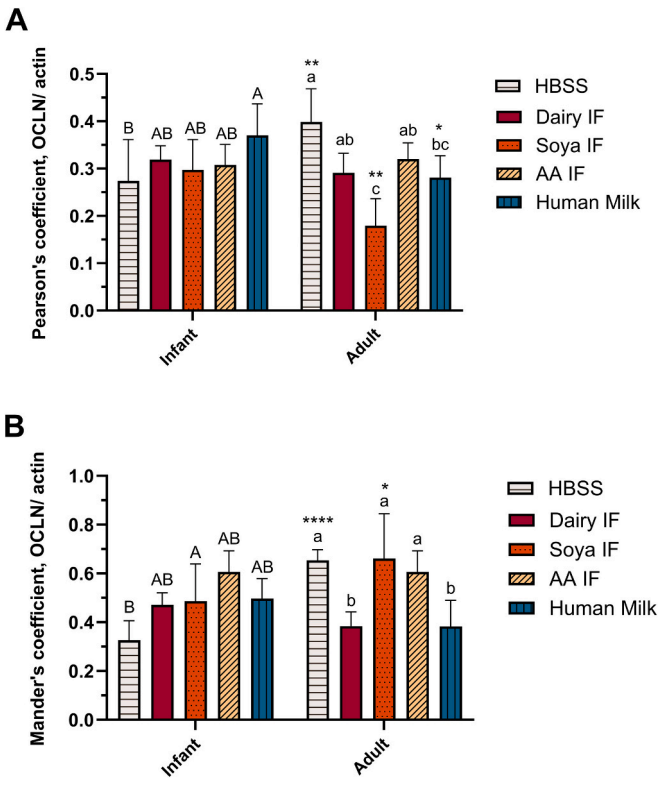

Fig. 4. Colocalization of occludin (OCLN) and actin in infant- and adult-like Caco-2/HT29-MTX monolayers exposed to digested infant formulas (IF) and Human Milk. Adult- and infant-like Caco-2/HT29-MTX (90:10) monolayers (day 25) were treated for 2 h with digested Dairy, Soya, or amino acid-based (AA) IF or Human Milk. Confocal images were analyzed in FIJI (ImageJ). (A) Pearson's coefficient quantifies overall OCLN–actin co-localization. (B) Manders' M1 coefficient shows the fraction of OCLN overlapping with actin. Data are mean ± SEM from three biological replicates (n = 9). One-way ANOVA with Tukey's test: different letters indicate differences between treatments within infant (uppercase) or adult (lowercase) models; asterisks indicate significant differences between infant and adult models ($P < 0.05$).

background levels were ~ 2-fold lower than the T2-basolateral free AA concentrations measured after exposure to digested dairy IF, soya IF, AA IF, and human milk (Fig. 5), indicating that the AAs detected in the transport experiments originated from the formulations rather than the buffer or cell system. Free AA in basolateral T2 samples were quantified by UHPLC–HRMS/MS (Supplementary Fig. 6). Supplementary Tables 2C and 2D also include UHPLC–HRMS/MS data for digesta samples for comparison purposes.

3.5. *Infant-like monolayers exhibit higher peptide transport and higher sequence diversity*

To identify peptides present post-digestion and post-absorption, UHPLC–HRMS/MS was performed in the digesta (I60), T2-apical and T2-basolateral samples for all foods (dairy IF, soya IF and human milk). Database searches were performed against custom UniProtKB FASTA files corresponding to *Bos taurus* (dairy), *Glycine* max (soya) or *Homo sapiens* (human milk), allowing only data comparisons between infant and adult-like monolayers.

Fig. 6 depicts total unique peptide counts in digesta, infant (A, C, E) and adult (B, D, F) models. Detailed counts of unique and shared peptides across digesta, T2- apical, and T2-basolateral samples for each formulation and model are provided in Supplementary Tables S3.

To define the baseline peptide pool available for epithelial interaction, digesta samples were first characterized for peptide abundance and physicochemical properties (Supplementary Tables S4). A total of 170, 229, and 129 unique peptides were identified in dairy IF, soya IF, and human milk digesta, respectively. Across all formulations, digesta peptides were predominantly short, with oligopeptides (4–10 amino acids) representing 61.17% of dairy IF, 61.14% of soya IF, and 75.19% of human milk peptides. In contrast, peptides longer than 20 amino acids accounted for ≤3.49% of the total in all cases. Consistently, human milk digesta peptides were primarily distributed within the 500–1000 Da range (55.04%), while the 1000–2000 Da range predominated in dairy IF (56.47%) and soya IF (56.33%). Hydrophobicity profiles differed between digesta samples. Dairy IF peptides were predominantly neutral (80.59%), with 17.06% hydrophilic and 2.35% hydrophobic peptides. Soya IF peptides showed a higher proportion of hydrophilic sequences (50.22%) and fewer neutral peptides (48.47%), with hydrophobic peptides remaining rare (1.31%). Human milk peptides displayed an intermediate profile, dominated by neutral peptides (67.44%), with

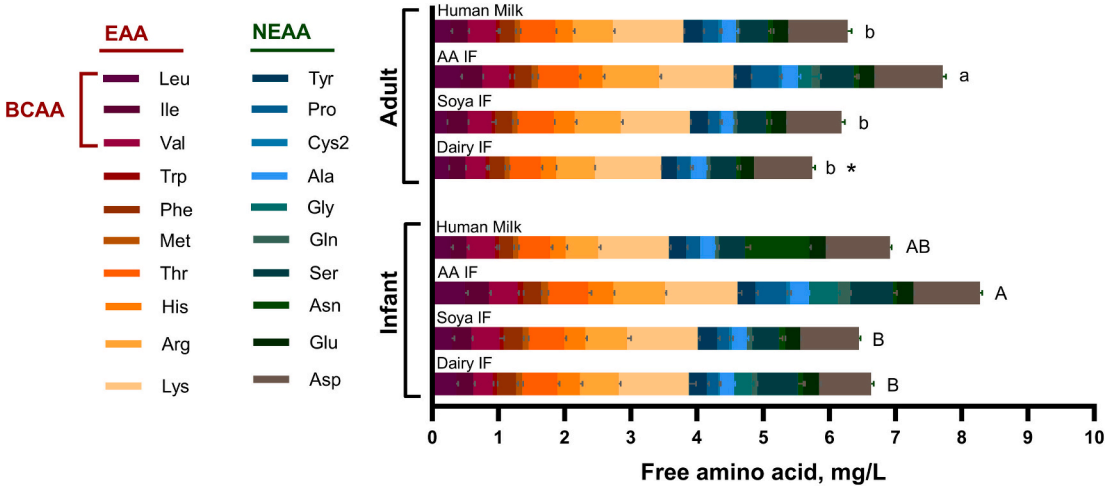

Fig. 5. Free Amino acid concentration in the basolateral compartments of Caco-2/HT29-MTX monolayers treated with digested Infant Formulas (IF) and Human Milk. Free amino acid concentrations (mg/L) in the basolateral compartment of infant-like and adult-like monolayers exposed for 2 h to digested Dairy IF, Soya IF, amino-acid (AA) IF, and Human Milk, measured by UHPLC-HRMS/MS. Data are mean ± SEM from three biological replicates (technical duplicates). One-way ANOVA with Tukey's test: different letters indicate differences between treatments within infant (uppercase) or adult (lowercase) models; asterisks indicate adult vs. infant differences ($P < 0.05$). Amino acids: red = BCAA, red + orange = EAA, blue/green = NEAA. (For interpretation of the references to colour in this figure legend, the reader is referred to the web version of this article.)

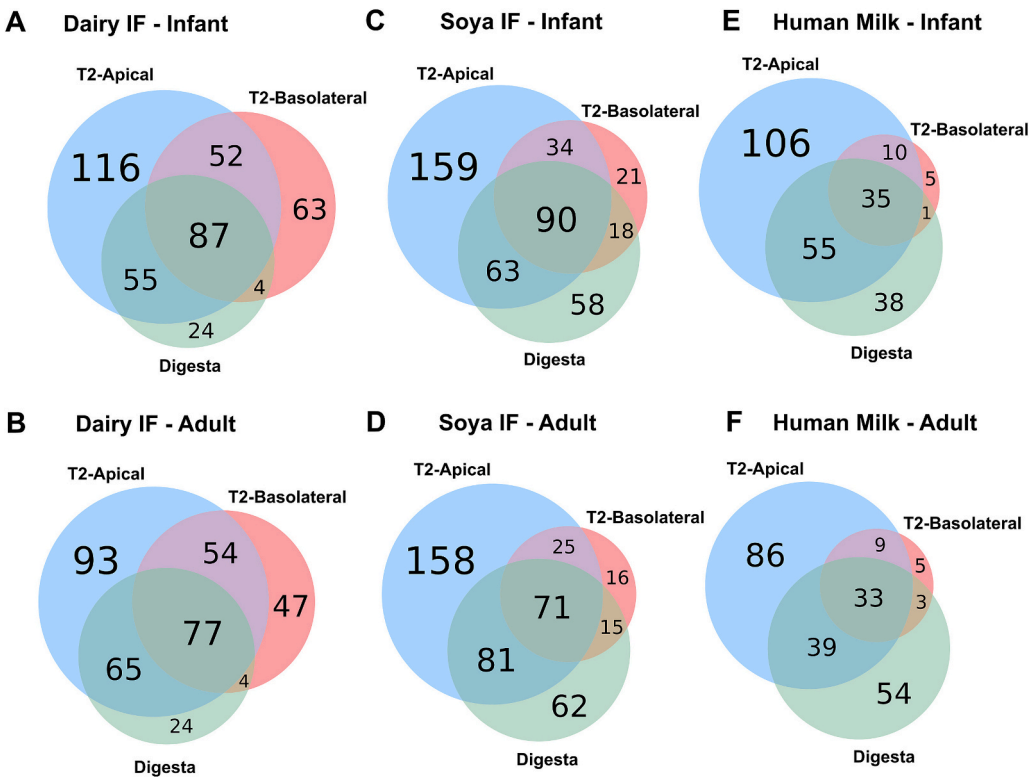

Fig. 6. Venn diagrams of unique peptides detected in infant- and adult-like monolayers treated with digested Dairy IF, Soya IF or Human Milk Infant- and adult-like monolayers were treated for 2 h (T2) with digested Dairy IF, Soya IF, or Human Milk. Peptides identified by UHPLC–HRMS/MS in digesta (green) compartments, in T2-apical (blue) and in T2-basolateral (red. Panels: (A–B) Dairy IF, (C—D) Soya IF, (E–F) Human Milk in infant and adult models. (For interpretation of the references to colour in this figure legend, the reader is referred to the web version of this article.)

28.68% hydrophilic and 3.88% hydrophobic peptides. Amino acid composition of the peptides revealed distinct but biologically consistent differences between digesta samples. Dairy IF and human milk digesta peptides were strongly enriched in proline (26.3% and 25.5%, respectively), whereas soya IF digesta contained a lower proportion of proline (17.0%). In contrast, soya digesta peptides showed a marked enrichment in acidic residues, with glutamic acid and aspartic acid together accounting for approximately 21.09% of total residues, compared with 11.70% in dairy IF and 9.89% in human milk digesta. Branched-chain amino acids (valine, leucine, and isoleucine) were more abundant in dairy IF and human milk digesta (23% and 22.96% respectively) than in soya IF digesta 15.03%), contributing to a higher proportion of neutral peptides. Human milk digesta further exhibited elevated glutamine content (11.6%).

Regarding peptides detected after epithelial exposure, differences in peptide diversity and compartmental overlap were assessed in infant- and adult-like models.

For dairy IF, 206 and 182 unique peptides were identified in the T2-basolateral compartments of infant- and adult-like models, respectively. In the T2-apical compartments, 310 unique peptides were detected in the infant model and 289 in the adult. In the infant model, 139 unique peptides were common to both T2-apical and T2-basolateral samples, 52 of which were absent from the digesta. In the adult monolayer treated with dairy IF digesta, the T2-apical and T2- basolateral samples had 131 peptides in common, of which 54 were not present in the digesta. Additionally, 67 peptides were found in the infant T2-basolateral compartment only (not detected in T2-apical or digesta), compared with 47 in the adult T2-basolateral compartment only.

For soya IF, the infant- and adult-like models yielded 163 and 127 unique peptides in the T2-basolateral compartment and 335 and 366 in the T2-apical compartment, respectively. Of these, 124 (infant) and 96 (adult) were shared across compartments, while 39 and 31 were in the T2-basolateral sample only. Thirty-four peptides (infant) and 25 (adult) were shared between apical and basolateral compartments but were not present in the digesta.

For human milk, the infant- and adult-like models yielded 206 and 167 unique peptides in the T2-apical compartment and 51 and 50 in the T2-basolateral compartment, respectively. Of these, 45 (infant) and 42 (adult) were shared across compartments. Notably, 10 (infant) and 8 (adult) of these shared peptides were absent from the digesta. Six (infant) and 8 (adult) peptides were found in the T2-basolateral side only.

To further characterize basolateral transport, physicochemical properties were analyzed in silico (Supplementary Table S5). In all matrices, the majority of transported peptides (>80% for dairy and 100% for soya and human milk) exceeded 3 AAs. Among peptides common to both models, median length was 7 AAs for dairy IF and 9 AAs for both soya IF and human milk. Among peptides exclusive to a single model, infant-exclusive dairy peptides were the shortest (median 4 AAs), whereas adult-exclusive soya peptides were the longest (median 13 AAs). Soya IF peptides exhibited more negative median charge and lower hydropathy values than dairy IF and human milk peptides. Infant-like monolayers consistently yielded a higher number of unique basolateral peptides across matrices.

Across all foods, the number of peptides identified in the T2-apical samples exceeded those in the original digesta. Moreover, each formula showed a subset of peptides shared between T2-apical and T2-basolateral compartments but absent from the digesta. Together, these findings suggest that brush border enzymes further cleave dietary peptides during the 2 h incubation, generating new fragments capable of transepithelial transport.

Interestingly, the peptides exclusive to the infant-like monolayer with dairy IF treatment had a lower median length (3.5 AAs) than those in the adult-like monolayer (4 AAs) and included a notably higher number of tripeptides (39 vs. 14 in adults). In contrast, peptides

exclusive to the infant-like monolayer with soya IF or human milk treatments were generally longer (soya IF: median infant = 9, adult = 8; human milk: median infant = 8, adult = 4.5), suggesting less hydrolysis.

3.6. Apical peptides reflect active brush border enzyme cleavage

With dairy IF, soya IF, and human milk treatments, a substantial number of unique peptides were detected in the T2-apical compartment that were not present in the digesta, suggesting further processing by epithelial peptidase enzymes. To explore whether the peptides identified in the apical compartment were a result of brush border enzyme activity, peptides present in the T2-apical chamber were assigned to parental digesta peptides with cleavage sites mapped to known intestinal brush border enzymes. Predicted brush border enzyme cleavage events and associated peptide origins are reported in Supplementary Tables S6. Fig. 7 illustrates the total number of times each brush border enzyme was involved in cleaving apical peptides, with higher event counts indicating greater predicted brush border activity. When including both 1-step and multi-step cleavage events, the infant-like model had 51 (dairy IF treatment), 61 (soya IF treatment), and 31 (human milk treatment) cleavage events. The adult-like model had 52 (dairy IF treatment), 59 (soya IF treatment), and 27 (human milk treatment) cleavage events. Tripeptidyl peptidase II, aminopeptidase N, and dipeptidyl peptidase-4 were the most commonly assigned brush border enzymes across all conditions, collectively accounting for the majority of predicted cleavage events.

In terms of peptide counts, the T2-apical sample collected with dairy IF treatment showed 36 single-step and 11 multi-step peptides in the infant-like model, compared to 36 single-step and 10 multi-step in the adult-like model. With soya-IF treatment, the T2-apical sample of infant monolayers had 41 single-step and 12 multi-step peptides, while the T2-apical sample from adult-like monolayers had 38 single-step and 12 multi-step peptides. With human milk treatment, the T2-apical sample of infant-like monolayers yielded 26 single-step and 4 multi-step peptides, compared with 22 and 4 in the T2-apical sample of adult-like model.

3.7. Infant-like monolayers show enhanced basolateral peptide load in response to human milk

To study the total load of peptides transported across the intestinal barrier, both the total peptide intensity (log_2-normalized) and the total number of peptides (including repeated detections of the same sequence) in T2-apical (Fig. 8A, B) and T2-basolateral (Fig. 8C, D) samples were quantified.

In the T2-basolateral compartment, both the total peptide intensity and count were significantly higher in the infant model treated with digested human milk compared to the adult model ($P < 0.05$). Peptide intensity was 30.10 ± 0.24 in infants versus 28.58 ± 0.22 in adults, and peptide count was 68.67 ± 0.67 vs. 60 ± 1, respectively. With dairy and soya IF treatments, no significant differences in peptide intensity or count were detected between infant and adult models on the T2-basolateral side ($P > 0.05$).

In the T2-apical compartment, no significant differences in peptide intensity (reflecting relative abundance) and count were observed between infant and adult monolayers for any of the food conditions ($P >$

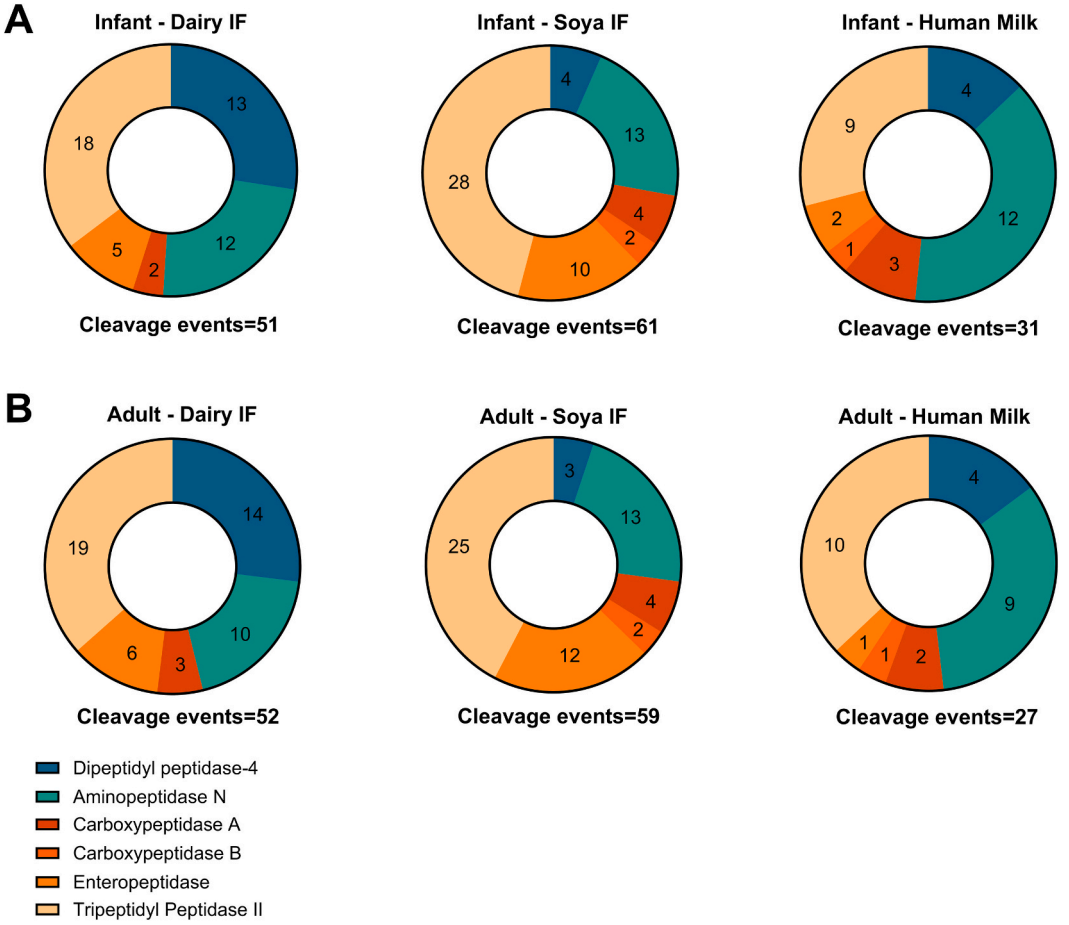

Fig. 7. Cleavage events attributed to specific brush border enzymes. (A) Infant-like and (B) adult-like Caco-2/HT29-MTX monolayers were treated for 2 h (T2) with digested Dairy IF, Soya IF, and Human Milk. Peptides identified in the T2-apical compartment (UHPLC–HRMS/MS) were compared with those in digesta to map new cleavage sites. Cleavage motifs were matched to specific enzymes, with higher event counts indicating greater predicted brush border activity.

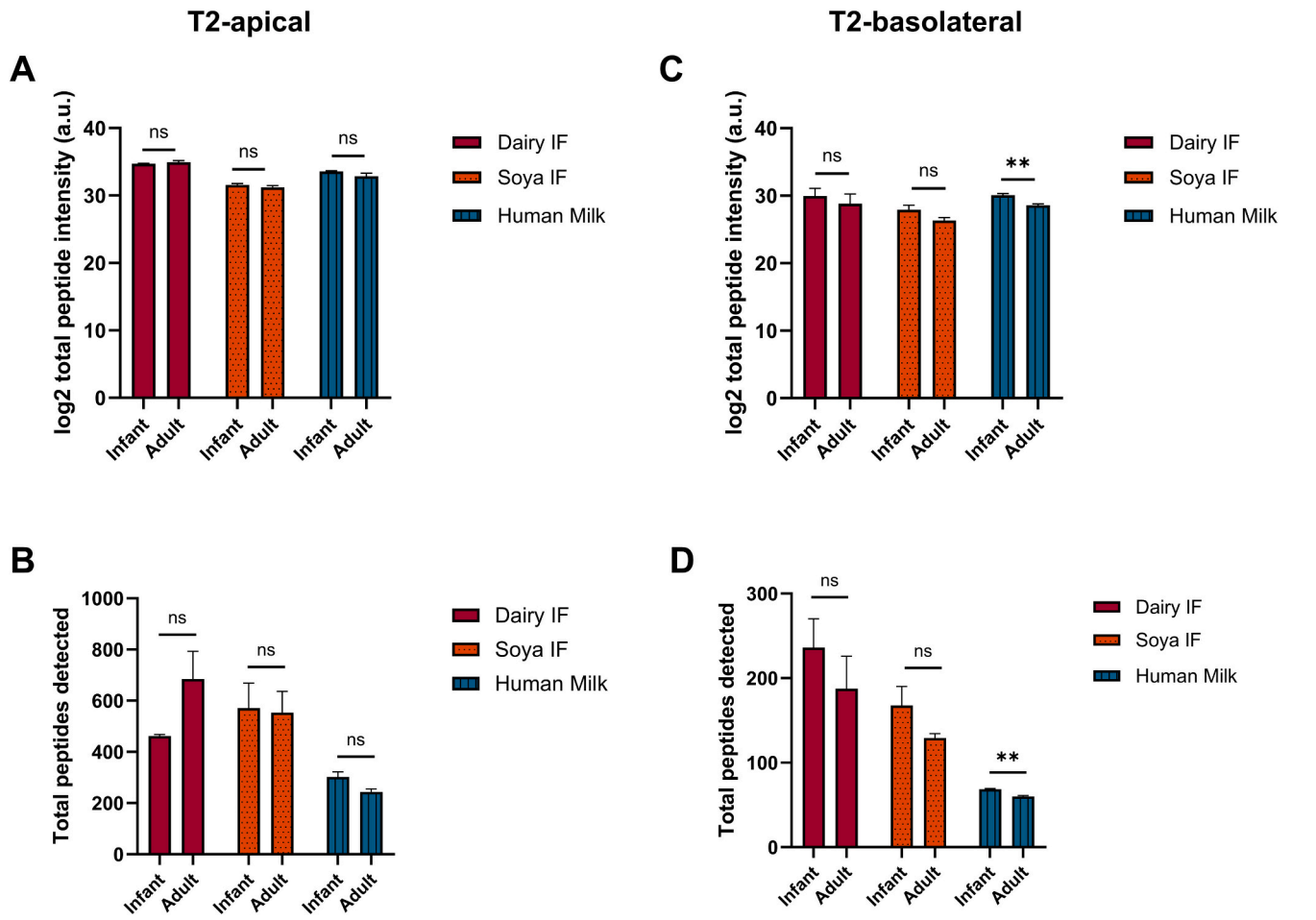

Fig. 8. Peptide transport across infant- and adult-like monolayers after exposure to digested infant formulas (IFs) and Human Milk. Infant-like and adult-like monolayers (day 25, Caco-2/HT29-MTX 90:10) were treated for 2 h (T2) with digested Dairy IF, Soya IF, and Human Milk. UHPLC–HRMS/MS was used to measure: (A, C) log_2-transformed total peptide intensity and (B, D) total peptide count in apical and basolateral compartments at T2. Data are mean ± SEM from three biological replicates. Unpaired *t*-tests compare infant and adult models; asterisks indicate significant differences ($P < 0.05$).

0.05).

3.8. *Human milk-derived bioactive peptides are more abundant in infant-like monolayers*

To assess whether peptides present in the T2-apical and T2-basolateral compartments exhibited bioactivity, PeptideRanker was employed to predict bioactivity scores based on sequence motifs (Mooney et al., 2012). The results were, matched against the BIOPEP and MBPD databases, which catalogue experimentally validated and predicted bioactive peptides. Fig. 9 displays volcano plots of log_2 intensity differences (infant – adult) for individual peptides, highlighting those with predicted or confirmed bioactivities. All identified bioactive peptides, their predicted functions, and statistical comparisons are reported in Supplementary Tables S7 (dairy IF), S8 (soya IF), S9 (human milk). Peptides with multiple predicted bioactivities were included in the count for each functional category to capture their multifunctional potential.

In the T2-apical compartment, monolayers treated with dairy IF yielded the highest number of bioactive peptides ($n = 86$), primarily linked to ACE inhibition ($n = 45$), antioxidative activity ($n = 21$), DPP-IV inhibition ($n = 12$), immunomodulation ($n = 11$), and AChE inhibition ($n = 8$). Among these, three peptides with antioxidant, DPP-IV inhibitory, and hypouricemic functions were more abundant in the infant model, while two antiamnestic and ACE-inhibitory peptides were higher in adult-like monoaleyrs. T2-apical samples from monolayers treated with human milk contained 11 bioactive peptides, mostly ACE inhibitors ($n = 6$) and DPP-II inhibitors ($n = 3$), with individual peptides also associated with antioxidant, anticancer, opioid, cholesterol-regulating, and growth-promoting activities ($n = 1$ each). Two ACE-inhibitory peptides were significantly higher in infant monolayers. T2-apical samples form monolayers treated with soya IF contained only one identified bioactive peptide with both ACE-inhibitory and antioxidant potential.

In the absorbed fraction (T2-basolateral), monolayers treated with dairy IF contained 54 bioactive peptides, with functional classifications including ACE inhibition ($n = 26$), antioxidant ($n = 14$), and DPP-IV inhibition ($n = 12$). One opioid peptide (β-casein ^{75}YPF^{77}) was more abundant in T2-basolateral from infant monolayers, while one ACE-inhibitory peptide (κ-casein ^{77}LPYP^{80}) was higher in adult T2-basolateral. T2-basolateral samples from monolayers treated with soya IF yielded a single antioxidant peptide (β -conglycinin ^{267}SLVNNDDRDS^{276}). T2-basolateral samples from monolayers treated with human milk contained five bioactive peptides: two with ACE-inhibitory activity, one with antioxidant activity, one with both ACE-inhibitory and antioxidant activity, and one with cholesterol-regulating activity. Notably, four of the five peptides were detected at significantly higher intensity in the infant model than in the adult ($P < 0.05$).

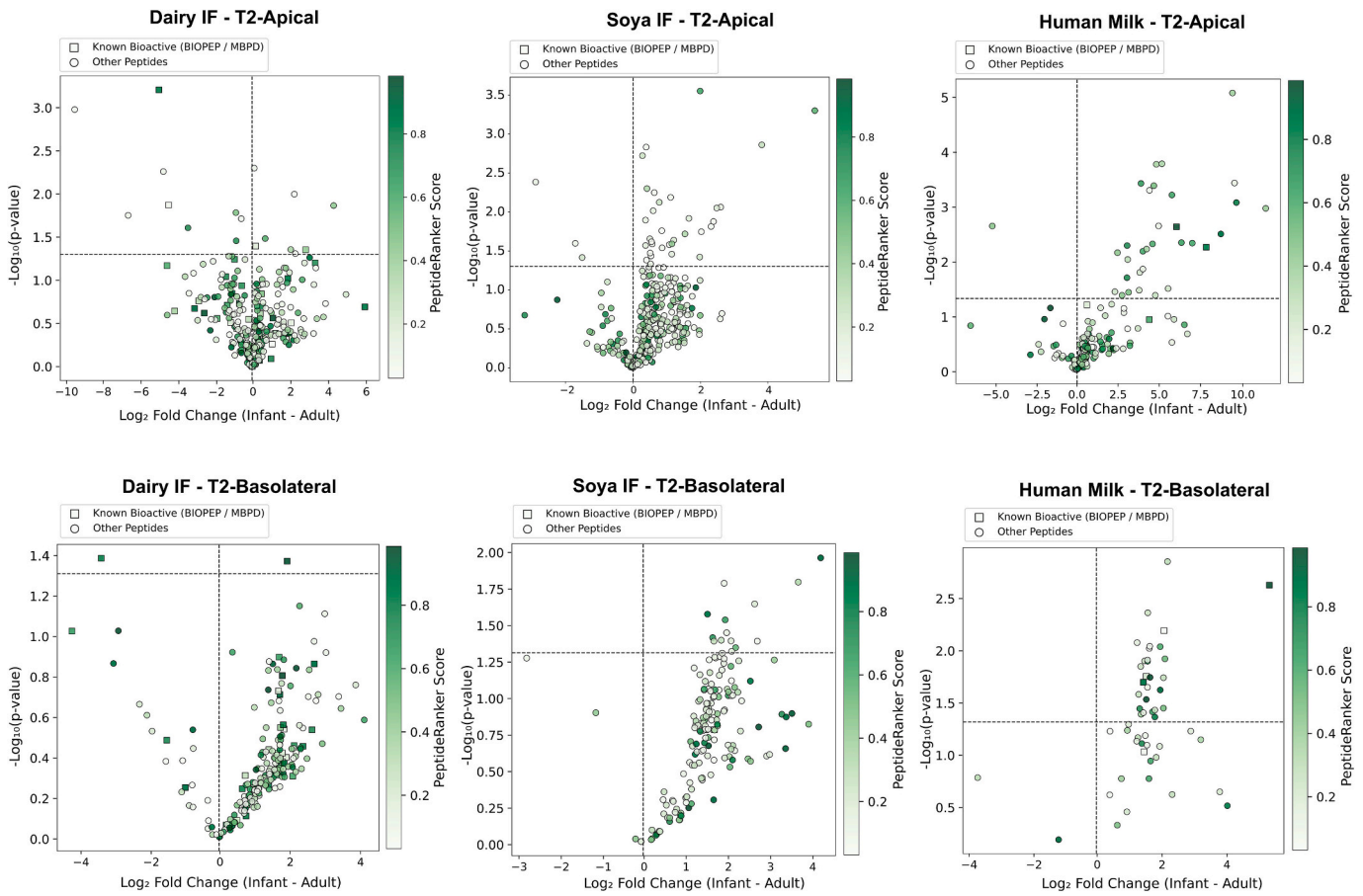

Fig. 9. Volcano plots of peptide abundance differences between infant- and adult-like models after exposure to digested infant formulas (IF) and Human Milk. Infant- and adult-like Caco-2/HT29-MTX monolayers were treated for 2 h (T2) with digested Dairy IF, Soya IF, and Human Milk. Peptides identified by UHPLC–HRMS/MS in the (A) T2-apical and (B) T2-basolateral samples are shown. Each point represents a peptide; X-axis = $\log_2$ fold change (infant − adult), Y-axis = $-\log_{10}$(*P*-value) from unpaired t-tests. Horizontal line indicates $P = 0.05$. The vertical line at $\log_2$ fold change = 0 separates peptides enriched in the infant model (right side, positive values) from those enriched in the adult model (left side, negative values). The upper-right quadrant highlights peptides significantly more abundant in infants, while the upper-left quadrant highlights peptides significantly more abundant in adults. Colour intensity reflects predicted bioactivity (PeptideRanker); darker green = higher bioactivity. Squares = peptides matched to known bioactive sequences (BIOPEP/MBPD), circles = unmatched peptides. (For interpretation of the references to colour in this figure legend, the reader is referred to the web version of this article.)

4. Discussion

In this study, infant- and adult-like Caco-2/HT29-MTX models were treated with gastrointestinal digests of human milk, dairy IF, soya IF or AA IF. The main findings were (i) human milk uniquely enhanced OCLN–actin co-localization and increased basolateral bioactive peptides in the infant-like model, (ii) IFs showed limited effects on both models, with AA–based formula increasing OCLN intensity in infant-like monolayers whilst lowering TEER in adult-like monolayers, and (iii) dietary peptide transport and diversity were consistently higher in infant- than adult-like models, highlighting the value of age-appropriate systems for infant nutrition research.

The primary finding for human milk was that treatment of the infant-like monolayer resulted in significantly increased OCLN/actin co-localization (Fig. 4, $P < 0.05$), indicating tight junction remodeling despite no overall change in OCLN expression or TEER values (Fig. 2; $P > 0.05$). Confocal imaging confirmed brighter OCLN staining at intercellular junctions. Importantly, these effects were unique to the infant-like model and absent in the adult-like condition. OCLN participates in maintaining epithelial barrier function by modulating paracellular permeability and coordinating tight junction assembly through its interactions with cytoplasmic adaptors (e.g., ZO1) and the actin cytoskeleton (Cummins, 2012). Because OCLN is physically anchored to the perijunctional actin ring via scaffold proteins, its spatial organization is inherently linked to actin architecture. Therefore, changes in OCLN–actin co-localization reflect remodeling of tight junction structural organization. Given that actin is broadly distributed throughout the cytoplasm while OCLN is confined to junctional regions, complete pixel overlap is not expected; thus, moderate Pearson's coefficient values are consistent with tight junction biology.

The age-specific difference in OCLN–actin co-localization may reflect differences in intracellular signaling between models. In our previous work, we showed that the GDC-induced infant-like monolayer exhibits reduced intracellular cAMP levels via TGR5–Gαi signaling, associated with altered tight junction organization (Bietto et al., 2025). Because cAMP signaling regulates tight junction organization, reduced baseline cAMP in the infant-like model may contribute to the enhanced OCLN redistribution following exposure to human milk.

These structural changes observed in our infant-like model are interesting in the context of Noel et al. study, who reported that human colostrum induced a granular OCLN pattern in pediatric enteroids, particularly co-localizing with goblet (trefoil factor 3 +) and Paneth (lysozyme +) cells (Noel et al., 2021). Kondrashina et al. (2024) observed no OCLN upregulation ($P > 0.05$) after 4 h exposure to digested human milk and dairy IF (500 μg/cm^2) in Caco-2/HT29-MTX monolayers, although TEER was significantly increased compared with HBSS controls (664 ± 72 Ω·cm^2; $P < 0.05$) (Kondrashina et al., 2024). Kondrashina et al. used an adult-like Caco-2/HT29-MTX model,

whereas our study and that of Noel et al. employed infant-like or pediatric enteroid systems, which may better capture age-specific responses. Although human milk is complex, the peptide and AA profiles post-gastrointestinal digestion may play a role in this OCLN response. SEC revealed large proteins/peptides remaining) at the end of the intestinal phase (MW > 50 kDa-Fig. 1B). SDS-PAGE had a persistent ~80 kDa band likely to be glycosylated lactoferrin, known to be resistant to digestion (Ma et al., 2021; Van Berkel et al., 1995). Lactoferrin has been shown to improve gut barrier function directly, exerting its biological effects in the gut lumen (Conesa et al., 2023). Also, in Caco-2 monolayers, Zhao et al. (2019) demonstrated that treatment with bovine lactoferrin significantly increased both mRNA and protein levels of OCLN and promoted its redistribution to the cell membrane, as shown by immunofluorescence (Zhao et al., 2019). Importantly, there is currently no evidence to support efficient transepithelial transport of intact lactoferrin in term infants (Mastromarino et al., 2014; Scott, 1989). Consistent with in vivo data, no lactoferrin-derived peptides were detected in the basolateral compartment of our Caco-2/HT29-MTX barrier. However, our analytical approach is optimized for low–molecular-weight peptide profiling and does not enable assessment of intact protein uptake.

In addition to lactoferrin, digested human milk contained significantly higher levels of free glutamic acid. In vitro, glutamic acid improves TEER in infant pig IPEC-J2 monolayers (0.5 mmol/L) (Jiao et al., 2015). As both a precursor and product of glutamine, glutamic acid also contributes indirectly to gut barrier maturation, since glutamine upregulates tight junction proteins (OCLN, CLDN1/4, ZO1/2/3) and restores barrier integrity (improved TEER and reduced ^{14}C-mannitol and FITC-dextran flux) in Caco-2 monolayers (Kim & Kim, 2017).

Peptide profiling of human milk revealed greater T2-basolateral transport and diversity in the infant- compared to the adult-like model (51 vs. 50 unique T2-basolateral peptides, UHPLC–HRMS/MS intensity 30.10 ± 0.24 $\log_2$ vs. 28.58 ± 0.22; total counts 68.67 ± 0.67 vs. 60.00 ± 1.00; Figs. 6 and 8; $P < 0.05$). The T2-apical compartment yielded 206 unique milk peptides for the infant and 167 for the adult. Previously, Liang et al. (2022) identified 169 peptides in the apical chamber and 44 peptides in the basolateral chamber after applying a digested human milk extract (10 μg/mL) to Caco-2 monolayers for 12 h. There was overlap with our data, including β-casein ^{138}NLHLPLP^{144} (ACE-inhibitory activity) and additional β-casein fragments such as ^{126}FDPQIPK^{132}, ^{210}PVTQPLAPV^{220}, and ^{96}PEIMEVPKA^{104}. In contrast, Kondrashina et al. (2024) reported only 17 basolateral peptides after 4 h exposure to human milk, of which 6 were common to our study. In terms of peptide abundance in the T2-basolateral compartment, the most abundant peptide for human milk was β-casein ^{126}FDPQIPK^{132} (1.17-fold higher in the infant-like model; $P > 0.05$), followed by β-casein ^{176}VLPIPQ^{181} (1.06-fold higher in the infant-like model; $P < 0.05$), with proven in vitro ACE-inhibitory effects (Kohmura et al., 1989). Notably, T2-basolateral peptides from the infant-like model carried a higher functional load. Five bioactive peptides were identified, four of which were more abundant in the infant-like condition. These included β-casein ^{176}VLPIPQ^{181}, β-casein ^{138}NLHLPLP^{144}, and β-casein ^{169}WSVPQPK^{175}, all exhibiting ACE-inhibitory activity (Hernández-Ledesma et al., 2007; Kohmura et al., 1989), as well as β-casein ^{90}VLPVPQ^{95}, which has been linked to cholesterol-regulating activity (Jiang et al., 2020). Interestingly, ^{169}WSVPQPK^{175} was also found in the gastric digesta of in vivo infants (Nielsen et al., 2018).

For the IF foods, no significant differences were observed in the response of infant-like monolayers to either dairy IF or soya IF, in terms of TEER (Fig. 2), OCLN intensity (Fig. 3), and OCLN/β-actin Pearson's co-localization coefficient (Fig. 4; $P < 0.05$). Consistent findings to our study were also reported by our group previously, where dairy IF digesta did not significantly alter TEER or OCLN levels in Caco-2/HT29-MTX monolayers (Dold et al., 2025). Similarly, Paparo et al. (2021) demonstrated that soya IF digesta did not impair TEER in Caco-2 cells, although it did upregulate OCLN mRNA expression (Paparo et al., 2021).

Notably, AA IF elicited a distinct response in the infant-like model: it significantly increased OCLN fluorescence intensity (Fig. 3B; $P < 0.05$) without a corresponding rise in TEER (Fig. 1A; $P > 0.05$) compared to HBSS. This may suggest that treatment with AA IF causes a selective tightening of the OCLN-regulated leak pathway, while the ion-conductive pore pathway that determines TEER remained unaffected (Al-Sadi et al., 2011). This finding aligns with in vivo data showing that extensively hydrolyzed formulas (no intact proteins) reduce intestinal paracellular permeability in infants (lactulose/mannitol ratio, $P = 0.003$) compared with conventional cow's milk-based formula (Koivusaari et al., 2023). In contrast, Paparo et al. (2021) found no upregulation of OCLN mRNA nor differences in TEER with AA IF in Caco-2 cells.

In the adult-like model, barrier responses to formula digesta diverged from the infant-like phenotype. Dairy IF reduced OCLN fluorescence intensity and Mander's coefficient for OCLN–actin co-localization (Fig. 3B and 4B; $P < 0.05$), Soya IF decreased Pearson's coefficient for OCLN–actin spatial correlation (Fig. 3A; $P < 0.05$), and AA IF significantly lowered TEER (Fig. 2B; $P < 0.05$) without affecting OCLN intensity (Fig. 3; $P > 0.05$). The TEER reduction observed with AA IF may reflect increased amino acid transport activity, as amino acid uptake is coupled to proton and ion fluxes (Bröer, 2008) that transiently influence TEER. This interpretation is supported by the higher basolateral amino acid levels measured in AA IF compared with those in the other samples ($P < 0.05$).

In terms of unique dairy or soya peptides transported to the T2-basolateral compartment, the infant-like monolayers consistently exhibited higher unique peptide counts (Fig. 6). For the dairy IF, we identified 206 unique peptides in the T2-basolateral and 314 in the T2-apical compartments for the infant-like model and 182 and 289 for the adult-like model. Similarly, Bavaro et al. (2021) identified 105 unique peptides in the basolateral and 585 in the apical compartments following 4 h exposure to 200 μg protein/cm^2 of digested heat-treated dairy infant formula (Bavaro et al., 2021). Of these, 132 apical peptides and 25 basolateral peptides matched to our data. In contrast, Kondrashina et al. (2024) identified only 17 peptides in the T2-basolateral side of Caco-2/HT29-MTX monolayers exposed for 4 h to dairy IF (Kondrashina et al., 2024). From their dataset, we identified 11 peptides in common from dairy IF (distributed across both compartments). In a milk protein study, Zenker et al. (2020) treated Caco-2 monolayers with gastrointestinal digested micellar casein and whey (80:20) for 2 h (Zenker et al., 2020). Assessment of milk peptide transport revealed 181 peptides on the basolateral side, including several peptides exhibiting sIgE-binding epitopes. When comparing their dataset with ours, we found four epitope-containing peptides in common—β-casein ^{98}VVPPFLQPE^{106}, ^{96}PVVVPPFLQPEV^{107}, ^{98}VVPPFLQPEV^{107}, and β-lactoglobulin ^{58}YVEELKPTPEGDLE^{71}. These bovine milk peptides were detected in both T2-apical and T2-basolateral compartments but absent in the digesta. With dairy IF treatment the most abundant peptide in the infant model was β-lactoglobulin ^{59}VEELKPTPE^{67} (1.04-fold higher in the infant model; $P > 0.05$), followed by β-casein ^{88}NIPPLTQTPV^{97} (1.08-fold higher; $P > 0.05$), which is also known for its ACE-inhibitory activity (Gobbetti et al., 2000). While dairy IF treatment produced the highest number of total bioactive peptides in the Transwell chambers (54 in T2-basolateral, 86 in T2-apical), these were more evenly distributed between models.

Where the infant-like model was treated with digested soya IF, 163 soya unique peptides were identified in the T2-basolateral and 346 in the T2-apical peptides. For the adult-like model, 127 soya unique peptides were identified in the basolateral and 335 in the apical. Martineau-Côté et al. (2024) identified 17 peptides in the basolateral and 55 in the apical fractions after exposing Caco-2/HT29-MTX monolayers for 2 h to digested soy flour (2240 μg of peptide/mL). When comparing their dataset with ours, we found five peptides in common: β-conglycinin ^{86}EPQQPGEKEEDEDEQPRPI^{104} (detected in both our T2-basolateral and T2-apical compartments), and seed linoleate

9S-lipoxygenase ^{208}NDLGDPDKGENH^{219}, Glycinin G4 ^{309}EQDEDEDEDEDKPRPS^{324} and ^{278}EEEEEEEDEKPQ^{287}, and sucrose-binding protein ^{309}TEVGPDDDEK^{338} (detected in our T2-apical compartment). Notably, these peptides were absent from our soya IF digesta.

The most abundant soya peptides in the Transwell chambers were glycinin ^{263}SVIKPPTDEQ^{272} (1.07-fold higher in the infant-like model; $P > 0.05$) and β-conglycinin ^{578}FVDAQPK^{584} (1.09-fold higher; $P > 0.05$).

Only one known bioactive peptide from soya was identified in the T2-apical compartment (Seed linoleate 13S-lipoxygenase-1 ^{306}TIIPLPV^{312}, ACE inhibitor and antioxidant (Minkiewicz et al., 2019)) and one in the T2-basolateral ^{267}β-conglycinin^{276} SLVNNDDRDS, antioxidant), with no significant difference between the infant and adult models ($P > 0.05$).

From our dataset, Caco-2/HT29-MTX brush border enzymes contributed to substantial protein digestion, as demonstrated by the higher number of peptides identified in the apical chamber after a 2 h incubation with monolayers but which were not present in the digesta (Fig. 7). In the infant model, 46 peptides from dairy IF, 53 from soya IF, and 30 from human milk matched cleavage motifs. The main enzymes implicated were tripeptidyl peptidase II, aminopeptidase N, and dipeptidyl peptidase-4, consistent with brush-border proteolytic activity. Similarly, Lacroix et al. (2017) studied five bioactive milk peptides and found that all underwent partial degradation by Caco-2 peptidases, with only ~70–90% remaining intact in the apical chamber after 2 h (Lacroix et al., 2017). Picariello et al. (2015) further showed that, after digestion of whey protein isolate, the addition of brush border enzymes from porcine jejunum increased the degree of hydrolysis from 53.3% to 70.7%, underscoring the crucial role of brush border enzymes in shaping the final peptide pool (Picariello et al., 2015).

Interestingly, peptides exclusively found in T2-apical of infant-like monolayers post-treatment with dairy-IF were shorter in length. This suggests more extensive cleavage by monolayer brush border enzymes or intracellular processing in response to dairy IF. This enhanced breakdown likely contributed to the higher T2-basolateral free AA levels observed in the infant-like condition compared with the adult model with dairy IF treatment.

The infant-like and adult-like barriers differed in their responses to the foods. Only the infant-like model responded to AA IF with increased OCLN fluorescence, and responded to human milk with enhanced OCLN–actin co-localization. By contrast, the adult model showed a reduction in TEER with AA IF treatment and lower OCLN fluorescence intensity with dairy IF and human milk treatments. Compared to the adult-like model, the infant-like monolayer also exhibited greater dietary peptide transport and diversity, with human milk in particular delivering a higher T2-basolateral load of bioactive peptides. Consistently, AA transport in the T2-basolateral was higher in the infant-like than in the adult-like model for dairy IF. These observations agree with in vivo data showing greater intestinal permeability in neonates, driven by enhanced paracellular transport (Catassi et al., 1995), a key route for peptide absorption (Xu et al., 2019). Thus, the adult Caco-2/HT29-MTX was less representative of the infant epithelium.

Interestingly, basolateral peptides across all dietary matrices exhibited a median length of 7–9 AAs, with the majority exceeding the di−/tri-peptide range that uses PepT1-mediated transport. This indicates that peptide passage across both infant- and adult-like epithelia is unlikely to be driven primarily by PepT1 and is consistent with a predominant contribution of paracellular permeability.

The overlap in basolateral peptide sequences between models suggests a conserved transport-permissive window for mid-length, moderately hydrophilic, and proline-enriched peptides. Notably, a higher number of infant-exclusive peptides were detected across matrices. This may reflect increased paracellular transport, consistent with developmental differences in epithelial maturation. Alternatively, differences in intracellular peptide degradation or transcytotic pathways may contribute to the observed infant-specific peptide profiles.

Limitations of this study include the absence of immune cells, short exposure windows, and a focus only on protein-derived bioactives. Additionally, peptide identification and bioactivity annotation are inherently limited by biases in available databases. Bovine milk proteins are overrepresented in proteomic and bioactive peptide databases compared to soya and human milk proteins. This may lead to an underestimation of peptide diversity or function in soya IF and human milk samples, and to an overrepresentation of bioactive hits in dairy IF. Expanding and diversifying peptide reference databases will be critical for accurate cross-formulation comparisons.

Barrier integrity was assessed using TEER (reflecting small-solute paracellular permeability) and quantitative OCLN–actin colocalization analysis. Moreover, basolateral peptides predominantly exceeded the size range typically transported by PepT1, suggesting a substantial contribution of paracellular permeability. While these approaches provide complementary functional and structural information, direct macromolecular permeability assays (e.g., FITC-dextran flux) and transporter perturbation or competitive inhibition studies would be required.

Future mechanistic studies are needed to determine the pathways underlying the OCLN–actin redistribution observed in response to human milk, including whether cAMP signaling contributes to this effect. Additional studies should assess long-term exposure effects, test lipid and carbohydrate fractions, and incorporate co-cultures with immune or mucus-producing cells. Nonetheless, our model offers a reproducible and efficient platform for early-life nutrition research.

5. Conclusions

In summary, the infant-like model revealed that digested human milk altered the architecture of tight junctions by increasing OCLN–actin co-localization and delivering a more diverse set of absorbed bioactive peptides. For all foods, infant-like monolayers transported more dietary peptides with greater diversity than the adult-like monolayers. For dairy IF, AAs levels in the T2-basolateral were higher in the infant-like than in the adult-like model. These observations align with in vivo data and support our view that in vitro barrier models that mimic the infant, should be used in conjunction with digestion protocols tailored to this life stage. Although both infant- and adult-like models showed similar responses to dairy- and soy-based IFs and human milk, the biomarkers assessed in this study were limited; therefore, future work should expand the biomarker panel. Nonetheless, formula development should prioritize more closely replicating the bioactive and barrier-supportive properties of human milk.

CRediT authorship contribution statement

Francesca Bietto: Writing – review & editing, Writing – original draft, Visualization, Validation, Methodology, Investigation, Formal analysis, Data curation, Conceptualization. **Simona Cirrincione:** Writing – review & editing, Methodology, Investigation, Formal analysis. **Cristina Gómez-Marín:** Writing – review & editing, Methodology, Investigation, Formal analysis. **Beatriz Miralles:** Writing – review & editing, Validation, Supervision, Resources, Methodology. **Francesco Romaniello:** Writing – review & editing, Methodology, Investigation, Formal analysis. **Elena Arranz:** Writing – review & editing, Supervision, Methodology. **Cristina Lamberti:** Writing – review & editing, Validation, Supervision, Resources. **Simona Lucia Bavaro:** Supervision, Resources, Methodology. **Laura Cavallarin:** Writing – review & editing, Supervision, Resources. **Eva Rath:** Writing – review & editing, Supervision, Methodology. **Alice J. Lucey:** Writing – review & editing, Validation, Supervision, Resources, Methodology. **Linda Giblin:** Writing – review & editing, Validation, Supervision, Resources, Project administration, Methodology, Funding acquisition, Conceptualization.

Ethics statement

Human milk was obtained from six healthy lactating women as part of a previously approved clinical study at the Hospital Universitario Virgen de las Nieves (Granada, Spain; Ethics Committee approval, ClinicalTrials.gov NCT02811172). All procedures complied with institutional guidelines and the Declaration of Helsinki. Written informed consent was obtained from all donors, including consent for future research use of their anonymized samples. Donor privacy and confidentiality were fully protected. No new human sample collection was performed for this study.

Declaration of competing interest

The authors declare that they have no known competing financial interests or personal relationships that could have appeared to influence the work reported in this paper.

Acknowledgments

This research was supported by Teagasc (InfBar MDBY1370). Francesca Bietto is in receipt of a Teagasc Walsh Scholarship 2021007. The graphical abstract was created in BioRender (Bietto, F.,2025; https://BioRender.com/yzbm1g7). The methodological flow chart was created in BioRender (Bietto, F., 2026; https://BioRender.com/p17zwmd). The authors would like to acknowledge Orla Cooney for proofreading this manuscript.

Appendix A. Supplementary data

Supplementary data to this article can be found online at https://doi.org/10.1016/j.foodres.2026.119071.

Data availability

Data will be made available on request.

References

Al-Sadi, R., Khatib, K., Guo, S., Ye, D., Youssef, M., & Ma, T. (2011). Occludin regulates macromolecule flux across the intestinal epithelial tight junction barrier. *American Journal of Physiology. Gastrointestinal and Liver Physiology, 300*(6), G1054–G1064. https://doi.org/10.1152/ajpgi.00055.2011

Atyeo, C., & Alter, G. (2021). The multifaceted roles of breast milk antibodies. *Cell, 184*(6), 1486–1499. https://doi.org/10.1016/j.cell.2021.02.031

Bavaro, S. L., Mamone, G., Picariello, G., Callanan, M. J., Chen, Y., Brodkorb, A., & Giblin, L. (2021). Thermal or membrane processing for infant milk formula: Effects on protein digestion and integrity of the intestinal barrier. *Food Chemistry, 347*, Article 129019. https://doi.org/10.1016/j.foodchem.2021.129019

Bietto, F., Arranz, E., Miralles, B., Gómez-Marín, C., Rath, E., Lucey, A. J., & Giblin, L. (2025). Using sodium glycodeoxycholate to develop a temporary infant-like gut barrier model, in vitro. *Frontiers in Nutrition, 12*, Article 1577369. https://doi.org/10.3389/fnut.2025.1577369

Biondi Ryan, M. R., Zukaitis, J., Sutantawong, S., & Dallas, D. C. (2025). Overall evidence for milk-derived proteins and peptides in blood after digestion: A systematic review. *Nutrition Reviews*. , Article nuaf118. https://doi.org/10.1093/nutrit/nuaf118

Blum, L. M. (1999). *At the breast: Ideologies of breastfeeding and motherhood in the contemporary United States*. Beacon Press.

Bode, L. (2012). Human milk oligosaccharides: Every baby needs a sugar mama. *Glycobiology, 22*(9), 1147–1162. https://doi.org/10.1093/glycob/cws074

Brockway, M., Daniel, A. I., Reyes, S. M., Gauglitz, J. M., Granger, M., McDermid, J. M., … Azad, M. B. (2024). Human milk bioactive components and child growth and body composition in the first 2 years: A systematic review. *Advances in Nutrition, 15*(1), Article 100127. https://doi.org/10.1016/j.advnut.2023.09.015

Bröer, S. (2008). Amino acid transport across mammalian intestinal and renal epithelia. *Physiological Reviews, 88*(1), 249–286. https://doi.org/10.1152/physrev.00018.2006

Carr, L. E., Virmani, M. D., Rosa, F., Munblit, D., Matazel, K. S., Elolimy, A. A., & Yeruva, L. (2021). Role of human milk bioactives on infants gut and immune health. *Frontiers in Immunology, 12*. https://doi.org/10.3389/fimmu.2021.604080

Catassi, C., Bonucci, A., Coppa, G. V., Carlucci, A., & Giorgi, P. L. (1995). Intestinal permeability. Changes during the first month: Effect of natural versus artificial feeding. *Journal of Pediatric Gastroenterology and Nutrition, 21*(4), 383–386. https://doi.org/10.1097/00005176-199511000-00003

Codex Alimentarius Commission. (1981). *Codex Alimentarius commission. Standard for infant formula and formulas for special medical purposes intended for infants (CXS 72–1981)*. Rome: FAO/WHO. Revised 2023. https://www.fao.org/fao-who-codexalimentarius/sh-proxy/es/?lnk=1&url=https%253A%252F%252Fworkspace.fao.org%252Fsites%252Fcodex%252FStandards%252FCXS%2B72-1981%252FCXS_072e.pdf.

Colaizy, T. T., Bartick, M. C., Jegier, B. J., Green, B. D., Reinhold, A. G., Schaefer, A. J., … Poulsen, J. (2016). Impact of optimized breastfeeding on the costs of necrotizing enterocolitis in extremely low birthweight infants. *The Journal of Pediatrics, 175*, 100–105.e2. https://doi.org/10.1016/j.jpeds.2016.03.040

Conesa, C., Bellés, A., Grasa, L., & Sánchez, L. (2023). The role of lactoferrin in intestinal health. *Pharmaceutics, 15*(6), 1569. https://doi.org/10.3390/pharmaceutics15061569

Cox, J., & Mann, M. (2008). *MaxQuant* (Version 2.6.6.0) [Computer software]. https://www.maxquant.org/.

Cummins, A. G., Steele, T. W., LaBrooy, J. T., & Shearman, D. J. (1988). Maturation of the rat small intestine at weaning: Changes in epithelial cell kinetics, bacterial flora, and mucosal immune activity. *Gut, 29*(12), 1672–1679. https://doi.org/10.1136/gut.29.12.1672

Cummins, P. M. (2012). Occludin: One protein, many forms. *Molecular and Cellular Biology, 32*(2), 242–250. https://doi.org/10.1128/MCB.06029-11

Dold, C. A., Sahin, A. W., Lawlor, P. G., Hickey, R. M., & Giblin, L. (2025). Employing membrane filtration technology during infant milk formula processing, will improve intestinal barrier function in vitro. *International Dairy Journal, 167*, Article 106283. https://doi.org/10.1016/j.idairyj.2025.106283

European Commission. (2016). Commission delegated regulation (EU) 2016/127 of 25 september 2015 supplementing regulation (EU) no 609/2013 as regards the specific compositional and information requirements for infant formula and follow-on formula and as regards requirements on information relating to infant and young child feeding. *Official Journal of the European Union, L25*, 1–29.

Gleeson, J. P., Fein, K. C., Chaudhary, N., Doerfler, R., Newby, A. N., & Whitehead, K. A. (2021). The enhanced intestinal permeability of infant mice enables oral protein and macromolecular absorption without delivery technology. *International Journal of Pharmaceutics, 593*, Article 120120. https://doi.org/10.1016/j.ijpharm.2020.120120

Gobbetti, M., Ferranti, P., Smacchi, E., Goffredi, F., & Addeo, F. (2000). Production of angiotensin-I-converting-enzyme-inhibitory peptides in fermented milks started by lactobacillus delbrueckii subsp. bulgaricus SS1 and lactococcus lactis subsp. cremoris FT4. *Applied and Environmental Microbiology, 66*(9), 3898–3904. https://doi.org/10.1128/AEM.66.9.3898-3904.2000

Google Research (2026). Google Colaboratory [Computer software]. Retrieved https://colab.research.google.com/.

Grundy, M. M.-L., Deglaire, A., Le Feunteun, S., Reboul, E., Moughan, P. J., Wilde, P. J., … Marze, S. (2025). Bioaccessibility and associated concepts: Terminology in the context of in vitro food digestion studies. *Food Chemistry, 485*, Article 144424. https://doi.org/10.1016/j.foodchem.2025.144424

Harris, C. R., Millman, K. J., Van Der Walt, S. J., Gommers, R., Virtanen, P., Cournapeau, D., … Oliphant, T. E. (2020). Array programming with NumPy. *Nature, 585*(7825), 357–362. https://doi.org/10.1038/s41586-020-2649-2

Hernández-Ledesma, B., Quirós, A., Amigo, L., & Recio, I. (2007). Identification of bioactive peptides after digestion of human milk and infant formula with pepsin and pancreatin. *International Dairy Journal, 17*(1), 42–49. https://doi.org/10.1016/j.idairyj.2005.12.012

Hevia, A., Ruas-Madiedo, P., Faria, M. A., Petit, V., Alves, B., Alvito, P., … Miralles, B. (2023). A shared perspective on in vitro and in vivo models to assay intestinal transepithelial transport of food compounds. *Journal of Agricultural and Food Chemistry, 71*(49), 19265–19276. https://doi.org/10.1021/acs.jafc.3c05479

Hidalgo, I. J., Raub, T. J., & Borchardt, R. T. (1989). Characterization of the human colon carcinoma cell line (caco-2) as a model system for intestinal epithelial permeability. *Gastroenterology, 96*(2), 736–749. https://doi.org/10.1016/S0016-5085(89)80072-1

Holmes, J. L., Van Itallie, C. M., Rasmussen, J. E., & Anderson, J. M. (2006). Claudin profiling in the mouse during postnatal intestinal development and along the gastrointestinal tract reveals complex expression patterns. *Gene Expression Patterns, 6*(6), 581–588. https://doi.org/10.1016/j.modgep.2005.12.001

Hubatsch, I., Ragnarsson, E. G. E., & Artursson, P. (2007). Determination of drug permeability and prediction of drug absorption in caco-2 monolayers. *Nature Protocols, 2*(9), 2111–2119. https://doi.org/10.1038/nprot.2007.303

Hunter, J. D. (2007). Matplotlib [computer software]. https://matplotlib.org/.

Jiang, X., Pan, D., Zhang, T., Liu, C., Zhang, J., Su, M., … Guo, Y. (2020). Novel milk casein–derived peptides decrease cholesterol micellar solubility and cholesterol intestinal absorption in caco-2 cells. *Journal of Dairy Science, 103*(5), 3924–3936. https://doi.org/10.3168/jds.2019-17586

Jiao, N., Wu, Z., Ji, Y., Wang, B., Dai, Z., & Wu, G. (2015). L-glutamate enhances barrier and antioxidative functions in intestinal porcine epithelial cells. *The Journal of Nutrition, 145*(10), 2258–2264. https://doi.org/10.3945/jn.115.217661

Johansson, M. E. V., Ambort, D., Pelaseyed, T., Schütte, A., Gustafsson, J. K., Ermund, A., … Hansson, G. C. (2011). Composition and functional role of the mucus layers in the intestine. *Cellular and Molecular Life Sciences, 68*(22), 3635. https://doi.org/10.1007/s00018-011-0822-3

Johnston, S. D., Smye, M., Watson, R. G. P., McMillan, S. A., Trimble, E. R., & Love, A. H. G. (2000). Lactulose-mannitol intestinal permeability test: A useful screening test for adult coeliac disease. *Annals of Clinical Biochemistry: International Journal of Laboratory Medicine, 37*(4), 512–519. https://doi.org/10.1177/000456320003700413

Kim, M.-H., & Kim, H. (2017). The roles of glutamine in the intestine and its implication in intestinal diseases. *International Journal of Molecular Sciences, 18*(5), 1051. https://doi.org/10.3390/ijms18051051

Kleiveland, C. R. (2015). Co-cultivation of caco-2 and HT-29MTX. *The Impact of Food Bioactives on Health*, 135–140.

Kohmura, M., Nio, N., Kubo, K., Minoshima, Y., Munekata, E., & Ariyoshi, Y. (1989). Inhibition of angiotensin-converting enzyme by synthetic peptides of human β-casein. *Agricultural and Biological Chemistry, 53*(8), 2107–2114. https://doi.org/10.1080/00021369.1989.10869621

Koivusaari, K., Niinistö, S., Nevalainen, J., Honkanen, J., Ruohtula, T., Koreasalo, M., … Virtanen, S. M. (2023). Infant feeding, gut permeability, and gut inflammation markers. *Journal of Pediatric Gastroenterology and Nutrition, 76*(6), 822–829. https://doi.org/10.1097/MPG.0000000000003756

Komatsu, Y., Wada, Y., Shibasaki, T., Kitamura, Y., Ehara, T., Nakamura, H., & Miyaji, K. (2024). Comparison of protein digestibility of human milk and infant formula using the INFOGEST method under infant digestion conditions. *British Journal of Nutrition, 132*(3), 351–358. https://doi.org/10.1017/S0007114524001260

Kondrashina, A., Mamone, G., Giblin, L., & Lane, J. A. (2024). Infant milk formula enriched in dairy cream brings its digestibility closer to human milk and supports intestinal health in pre-clinical studies. *Nutrients, 16*(18), 3065. https://doi.org/10.3390/nu16183065

Korhonen, H., & Pihlanto, A. (2006). Bioactive peptides: Production and functionality. *International Dairy Journal, 16*(9), 945–960. https://doi.org/10.1016/j.idairyj.2005.10.012

Kosek, M. N., Lee, G. O., Guerrant, R. L., Haque, R., Kang, G., Ahmed, T., … Network, the M.-E. (2017). Age and sex normalization of intestinal permeability measures for the improved assessment of enteropathy in infancy and early childhood: Results from the MAL-ED study. *Journal of Pediatric Gastroenterology and Nutrition, 65*(1), 31–39. https://doi.org/10.1097/MPG.0000000000001610

Lacroix, I. M. E., Chen, X.-M., Kitts, D. D., & Li-Chan, E. C. Y. (2017). Investigation into the bioavailability of milk protein-derived peptides with dipeptidyl-peptidase IV inhibitory activity using caco-2 cell monolayers. *Food & Function, 8*(2), 701–709. https://doi.org/10.1039/C6FO01411A

Liang, N., Kim, B. J., & Dallas, D. C. (2022). Bioavailability of peptides derived from the in vitro digestion of human milk assessed by caco-2 cell monolayers. *Journal of Agricultural and Food Chemistry, 70*(23), 7077–7084. https://doi.org/10.1021/acs.jafc.2c01246

Lucas, A., & Cole, T. J. (1990). Breast milk and neonatal necrotising enterocolitis. *The Lancet, 336*(8730–8731), 1519–1523. https://doi.org/10.1016/0140-6736(90)93304-8

Ma, Y., Hou, Y., Xie, K., Zhang, L., & Zhou, P. (2021). Digestive differences in immunoglobulin g and lactoferrin among human, bovine, and caprine milk following in vitro digestion. *International Dairy Journal, 120*, Article 105081. https://doi.org/10.1016/j.idairyj.2021.105081

Macierzanka, A., Mackie, A. R., Bajka, B. H., Rigby, N. M., Nau, F., & Dupont, D. (2014). Transport of particles in intestinal mucus under simulated infant and adult physiological conditions: Impact of mucus structure and extracellular DNA. *PLoS One, 9*(4), Article e95274. https://doi.org/10.1371/journal.pone.0095274

Martin, C., Ling, P.-R., & Blackburn, G. (2016). Review of infant feeding: Key features of breast milk and infant formula. *Nutrients, 8*(5), 279. https://doi.org/10.3390/nu8050279

Martineau-Côté, D., Achouri, A., Pitre, M., Karboune, S., & L'Hocine, L. (2024). Bioaccessibility and Antioxidant Activity of Faba Bean Peptides in Comparison to those of Pea and Soy after In Vitro Gastrointestinal Digestion and Transepithelial Transport across Caco-2 and HT29-MTX-E12 Cells. *J. Agric. Food Chem., 72*(32), 17953–17963. https://doi.org/10.1021/acs.jafc.4c02948

Mastromarino, P., Capobianco, D., Campagna, G., Laforgia, N., Drimaco, P., Dileone, A., & Baldassarre, M. E. (2014). Correlation between lactoferrin and beneficial microbiota in breast milk and infant's feces. *BioMetals, 27*(5), 1077–1086. https://doi.org/10.1007/s10534-014-9762-3

McKinney, W. (2010). Pandas (version 1.5.3) [computer software]. https://pandas.pydata.org/.

McNamara, J. (2023). XlsxWriter: A python module for creating excel XLSX files. [computer software]. https://github.com/jmcnamara/XlsxWriter.

Ménard, O., Bourlieu, C., De Oliveira, S. C., Dellarosa, N., Laghi, L., Carrière, F., … Deglaire, A. (2018). A first step towards a consensus static in vitro model for simulating full-term infant digestion. *Food Chemistry, 240*, 338–345. https://doi.org/10.1016/j.foodchem.2017.07.145

Minkiewicz, P., Iwaniak, A., & Darewicz, M. (2019). BIOPEP-UWM database of bioactive peptides: Current opportunities. *International Journal of Molecular Sciences, 20*(23), 5978. https://doi.org/10.3390/ijms20235978

Mooney, C., Haslam, N. J., Pollastri, G., & Shields, D. C. (2012). Towards the improved discovery and design of functional peptides: Common features of diverse classes permit generalized prediction of bioactivity. *PLoS One, 7*(10), Article e45012. https://doi.org/10.1371/journal.pone.0045012

Musa, M. A., Kabir, M., Hossain, M. I., Ahmed, E., Siddique, A., Rashid, H., … Haque, R. (2019). Measurement of intestinal permeability using lactulose and mannitol with conventional five hours and shortened two hours urine collection by two different methods: HPAE-PAD and LC-MSMS. *PLoS One, 14*(8), Article e0220397. https://doi.org/10.1371/journal.pone.0220397

Nielsen, P. M., Petersen, D., & Dambmann, C. (2001). Improved method for determining food protein degree of hydrolysis. *Journal of Food Science, 66*(5), 642–646. https://doi.org/10.1111/j.1365-2621.2001.tb04614.x

Nielsen, S. D., Beverly, R. L., Qu, Y., & Dallas, D. C. (2017). Milk bioactive peptide database: A comprehensive database of milk protein-derived bioactive peptides and novel visualization. *Food Chemistry, 232*, 673–682. https://doi.org/10.1016/j.foodchem.2017.04.056

Nielsen, S. D., Beverly, R. L., Underwood, M. A., & Dallas, D. C. (2018). Release of functional peptides from mother's milk and fortifier proteins in the premature infant stomach. *PLoS One, 13*(11), Article e0208204. https://doi.org/10.1371/journal.pone.0208204

Noel, G., In, J. G., Lemme-Dumit, J. M., DeVine, L. R., Cole, R. N., Guerrerio, A. L., … Pasetti, M. F. (2021). Human breast milk enhances intestinal mucosal barrier function and innate immunity in a healthy pediatric human enteroid model. *Frontiers in Cell and Developmental Biology, 9*, Article 685171. https://doi.org/10.3389/fcell.2021.685171

Pannaraj, P. S., Li, F., Cerini, C., Bender, J. M., Yang, S., Rollie, A., … Aldrovandi, G. M. (2017). Association between breast milk bacterial communities and establishment and development of the infant gut microbiome. *JAMA Pediatrics, 171*(7), 647. https://doi.org/10.1001/jamapediatrics.2017.0378

Paparo, L., Picariello, G., Bruno, C., Pisapia, L., Canale, V., Sarracino, A., … Berni Canani, R. (2021). Tolerogenic effect elicited by protein fraction derived from different formulas for dietary treatment of cows milk allergy in human cells. *Frontiers in Immunology, 11*, Article 604075. https://doi.org/10.3389/fimmu.2020.604075

Pedregosa, F. (2011). Scikit-learn (version 1.2.2) [computer software]. https://scikit-learn.org/.

Picariello, G., Miralles, B., Mamone, G., Sánchez-Rivera, L., Recio, I., Addeo, F., & Ferranti, P. (2015). Role of intestinal brush border peptidases in the simulated digestion of milk proteins. *Molecular Nutrition & Food Research, 59*(5), 948–956. https://doi.org/10.1002/mnfr.201400856

Python Software Foundation (2021). *Python Language Reference, Version 3.10* (Version 3.10) [Computer software].

Quigley, M., Embleton, N. D., Meader, N., & McGuire, W. (2024). Donor human milk for preventing necrotising enterocolitis in very preterm or very low-birthweight infants. *Cochrane Database of Systematic Reviews, 2024*(9). https://doi.org/10.1002/14651858.CD002971.pub6

Sánchez-Hernández, S., Théron, L., Jiménez-Barrios, P., Olalla-Herrera, M., Recio, I., & Miralles, B. (2021). Protein profile and simulated digestive behavior of breast milk from overweight and normal weight mothers. *Foods, 10*(4), 887. https://doi.org/10.3390/foods10040887

Sangild, P. T., Ney, D. M., Sigalet, D. L., Vegge, A., & Burrin, D. (2014). Animal models of gastrointestinal and liver diseases. Animal models of infant short bowel syndrome: Translational relevance and challenges. *American Journal of Physiology. Gastrointestinal and Liver Physiology, 307*(12), G1147–G1168. https://doi.org/10.1152/ajpgi.00088.2014

Scott, P. H. (1989). Enzyme immunoassay of lactoferrin in newborn term infants: Reference values and influence of diet. *Annals of Clinical Biochemistry: International Journal of Laboratory Medicine, 26*(5), 407–411. https://doi.org/10.1177/000456328902600505

Sun, H., Chow, E. C., Liu, S., Du, Y., & Pang, K. S. (2008). The caco-2 cell monolayer: Usefulness and limitations. *Expert Opinion on Drug Metabolism & Toxicology, 4*(4), 395–411. https://doi.org/10.1517/17425255.4.4.395

Tretyakov, K. (2012). Matplotlib-venn: A python library for plotting venn diagrams. [computer software]. https://github.com/konstantint/matplotlib-venn.

UNICEF, & W. H. O. (2003). *Global strategy for infant and young child feeding.* World Health Organization.

Van Berkel, P. H. C., Geerts, M. E. J., Van Veen, H. A., Kooiman, P. M., Pieper, F. R., De Boer, H. A., & Nuijens, J. H. (1995). Glycosylated and unglycosylated human lactoferrins both bind iron and show identical affinities towards human lysozyme and bacterial lipopolysaccharide, but differ in their susceptibilities towards tryptic proteolysis. *Biochemical Journal, 312*(1), 107–114. https://doi.org/10.1042/bj3120107

Vergauwen, H. (2015). The IPEC-J2 cell line. In K. Verhoeckx, P. Cotter, I. López-Expósito, C. Kleiveland, T. Lea, A. Mackie, … H. Wichers (Eds.), *The impact of food bioactives on health: In vitro and ex vivo models*. Springer. http://www.ncbi.nlm.nih.gov/books/NBK500147/.

Virtanen, P. (2020). SciPy (version 1.10.1) [computer software]. https://scipy.org/.

Waskom, M. (2021). Seaborn [computer software]. https://seaborn.pydata.org/.

Weaver, L. T., Laker, M. F., & Nelson, R. (1984). Intestinal permeability in the newborn. *Archives of Disease in Childhood, 59*(3), 236–241. https://doi.org/10.1136/adc.59.3.236

Weström, B., Arévalo Sureda, E., Pierzynowska, K., Pierzynowski, S. G., & Pérez-Cano, F.-J. (2020). The immature gut barrier and its importance in establishing immunity in newborn mammals. *Frontiers in Immunology, 11*. https://www.frontiersin.org/articles/10.3389/fimmu.2020.01153.

World Health Organization. (2014). *Global nutrition targets 2025: Breastfeeding policy brief*. World Health Organization. https://www.who.int/publications/i/item/WHO-NMH-NHD-14.7.

Xu, Q., Hong, H., Wu, J., & Yan, X. (2019). Bioavailability of bioactive peptides derived from food proteins across the intestinal epithelial membrane: A review. *Trends in Food Science & Technology, 86*, 399–411. https://doi.org/10.1016/j.tifs.2019.02.050

Zenker, H. E., Wichers, H. J., Tomassen, M. M. M., Boeren, S., De Jong, N. W., & Hettinga, K. A. (2020). Peptide release after simulated infant in vitro digestion of dry heated cows milk protein and transport of potentially immunoreactive peptides across the caco-2 cell monolayer. *Nutrients, 12*(8), 2483. https://doi.org/10.3390/nu12082483

Zhao, X., Xu, X.-X., Liu, Y., Xi, E.-Z., An, J.-J., Tabys, D., & Liu, N. (2019). The in vitro protective role of bovine lactoferrin on intestinal epithelial barrier. *Molecules, 24*(1), 148. https://doi.org/10.3390/molecules24010148